

**LOADING RATE EFFECT ON JOINT SHEAR  
STRENGTH OF SANDSTONES**

**Bunsupa Chokchai**



**A Thesis Submitted in Partial Fulfillment of the Requirements for the  
Degree of Master of Engineering in Geotechnology  
Suranaree University of Technology  
Academic Year 2012**

## ผลกระทบของอัตราการให้แรงต่อกำลังเฉือนของรอยแตกในหินทราย

นางสาวบุญสุภา โชคชัย



วิทยานิพนธ์นี้เป็นส่วนหนึ่งของการศึกษาตามหลักสูตรปริญญาวิศวกรรมศาสตรมหาบัณฑิต

สาขาวิชาเทคโนโลยีธรณี

มหาวิทยาลัยเทคโนโลยีสุรนารี

ปีการศึกษา 2555

# LOADING RATE EFFECT ON JOINT SHEAR STRENGTH OF SANDSTONES

Suranaree University of Technology has approved this thesis submitted in partial fulfillment of the requirements for a Master's Degree.

Thesis Examining Committee

---

(Assoc. Prof. Kriangkrai Trisarn)

Chairperson

---

(Assoc. Prof. Dr. Kittitep Fuenkajorn)

Member (Thesis Advisor)

---

(Dr. Decho Phueakphum)

Member

---

(Prof. Dr. Sukit Limpijumnong)

Vice Rector for Academic Affairs

---

(Assoc. Prof. Ft. Lt. Dr. Kontorn Chamniprasart)

Dean of Institute of Engineering

บุญสุภา โชคชัย: ผลกระทบของอัตราการให้แรงต่อกำลังเฉือนของรอยแตกในหินทราย  
(LOADING RATE EFFECT ON JOINT SHEAR STRENGTH IN SANDSTONES)

อาจารย์ที่ปรึกษา: รองศาสตราจารย์ ดร.กิตติเทพ เฟื่องขจร, 51 หน้า

วัตถุประสงค์ของงานวิจัยนี้คือเพื่อศึกษาผลกระทบของอัตราการให้แรงเฉือนต่อค่ากำลังรับแรงเฉือนและค่าความเหนียวของรอยแตกของหินทราย โดยหินที่ใช้ในการทดสอบเป็นหินจากชุดหินทรายพระวิหาร ภูกระดึง และภูพาน ซึ่งเป็นชุดหินทรายที่พบได้มากในภาคตะวันออกเฉียงเหนือของประเทศไทย มีขนาดเม็ดหินที่ละเอียดมีความเป็นเนื้อเดียวกันและมีความหนาแน่นสูง รอยแตกของตัวอย่างหินทำขึ้นในห้องปฏิบัติการโดยวิธีการให้แรงกดแบบแนวเส้นเพื่อให้เกิดแรงดึงในตัวอย่างหิน พื้นที่หน้าตัดของรอยแตกที่ใช้ในการทดสอบมีขนาด  $10 \times 10$  ตารางเซนติเมตรและใช้หินแต่ละชนิดอย่างน้อยชนิดละ 25 ตัวอย่าง ขั้นตอนการทดสอบและวิธีการคำนวณปฏิบัติตามมาตรฐาน ASTM โดยให้แรงกดตั้งฉากกับรอยแตกคงที่ผันแปรจาก 0.2, 1, 2, 3 และ 4 เมกกะปาสคาล และใช้อัตราการเฉือนผันแปรจาก  $2 \times 10^{-5}$  ถึง  $2 \times 10^{-1}$  เมกกะปาสคาลต่อวินาที ผลการวิจัยที่ได้สำหรับหินทรายทั้งหมดที่ใช้ในการทดสอบพบว่าค่ากำลังรับแรงเฉือนสูงสุด ค่ากำลังรับแรงเฉือนคงเหลือและค่าความเหนียวของรอยแตกเพิ่มขึ้นแบบเอกซ์โพเนนเชียลกับอัตราการให้แรง โดยเฉพาะอย่างยิ่งภายใต้สภาวะความเค้นกดตั้งฉากสูง อัตราการเฉือนจะไม่มีผลกระทบกับมุมเสียดทานพื้นฐานของรอยแตกที่มีพื้นผิวเรียบ ค่าความเค้นยึดติดจะมีค่าเข้าใกล้ศูนย์ที่อัตราการเฉือน  $2 \times 10^{-5}$  เมกกะปาสคาลต่อวินาทีและมีค่าประมาณ 0.5-0.6 เมกกะปาสคาลที่อัตราการเฉือน  $2 \times 10^{-1}$  เมกกะปาสคาลต่อวินาที ส่วนค่ามุมเสียดทานจะมีค่าเพิ่มขึ้นประมาณ 5 องศา เมื่ออัตราการเฉือนเพิ่มขึ้นจาก  $2 \times 10^{-5}$  ถึง  $2 \times 10^{-1}$  เมกกะปาสคาลต่อวินาทีผลการวิจัยสามารถนำไปใช้ในการวิเคราะห์และออกแบบโครงสร้างทางวิศวกรรมในมวลหินที่รอยแตกอาจได้รับผลกระทบจากอัตราการเกิดแรงที่แตกต่างกันซึ่งเกิดขึ้นจากการเกิดแผ่นดินไหว การขุดเจาะและกิจกรรมจากการทำเหมือง

BUNSUPA CHOKCHAI : LOADING RATE EFFECT ON JOINT SHEAR  
STRENGTH OF SANDSTONES. THESIS ADVISOR: ASSOC. PROF.  
KITTITEP FUENKAJORN, Ph.D., P.E., 51 PP.

#### SHEAR STIFFNESS/NORMAL STIFFNESS/SHEAR STRENGTH/LOADING RATE

The objective of this study is to experimentally determine the effects of shear rate on the joint shear strengths and stiffness of fractures sandstone specimens prepared from the Phra Wihan, Phu Phan and Phu Kradung formations. These rocks are classified as fine-grain quartz sandstones with highly uniform texture and density. The fractures are artificially made in the laboratory by tension inducing method. The fracture area is  $10 \times 10 \text{ cm}^2$ . A minimum of 25 specimens are prepared for each sandstone type. The test procedure and method of calculation follow the ASTM standard practice. The normal stresses are maintained constant at 0.2, 1, 2, 3 and 4 MPa. The shear rates are varied from  $2 \times 10^{-5}$  to  $2 \times 10^{-1}$  MPa/s. The results indicate that for all sandstone types the peak and residual shear strengths and joint shear stiffness increase exponentially with loading rate, particularly under high normal stresses. The shear rate has no effect on the basic friction angle of the smooth saw-cut surfaces. The cohesion can be as low as zero under the shear rate of  $2 \times 10^{-5}$  MPa/s to about 0.5-0.6 MPa under the shear rate of  $2 \times 10^{-1}$  MPa/s. The friction angles can increase by about 5 degrees when the shear rates increase from  $2 \times 10^{-5}$  to  $2 \times 10^{-1}$  MPa/s. The findings are applicable to the analysis and design of

engineering structures in rock mass where the joints are subjected to different loading rates induced by seismic, excavation and mining activities.



School of Geotechnology

Academic Year 2010

Student's Signature\_\_\_\_\_

Advisor's Signature\_\_\_\_\_

## ACKNOWLEDGEMENTS

The author wishes to acknowledge the support from the Suranaree University of Technology (SUT) who has provided funding for this research.

Grateful thanks and appreciation are given to Assoc. Prof. Dr. Kittitip Fuenkajorn, thesis advisor, who lets the author work independently, but gave a critical review of this research. Many thank are also extended to Asst. Prof. Kriangkrai Trisarn and Dr. Prachaya Tepnarong, who served on the thesis committee and commented on the manuscript.

Finally, I most gratefully acknowledge my parents and friends for all their supported throughout the period of this research.

Bunsupa Chokchai

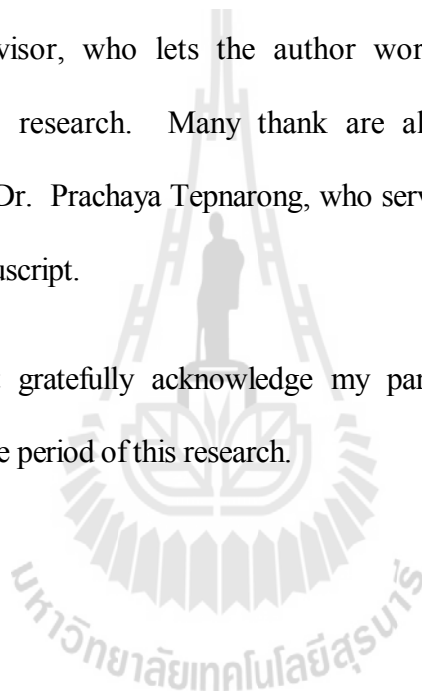


# TABLE OF CONTENTS

	<b>Page</b>
ABSTRRACT (THAI).....	I
ABSTRACT (ENGLISH).....	II
ACKNOWLEDGEMENTS .....	IV
TABLE OF CONTENTS.....	V
LIST OF TABLES.....	IX
LIST OF FIGURES .....	X
LIST OF SYMBOLS AND ABBREVIATIONS.....	XIV
<b>CHAPTER</b>	
<b>I INTRODUCTION.....</b>	<b>1</b>
1.1 Background of problems and significance of the study .....	1
1.2 Research objectives.....	1
1.3 Research methodology .....	2
1.3.1 Literature review.....	3
1.3.2 Sample collection and preparation.....	4
1.3.3 Development of true triaxial load frame .....	4
1.3.4 Calibration of true triaxial load frame .....	4
1.3.5 Laboratory experiments .....	4
1.3.6 Comparisons.....	5
1.3.7 Conclusions and thesis writing.....	5



## TABLE OF CONTENTS (Continued)

	<b>Page</b>
1.4 Scope and limitations of the study .....	5
1.5 Thesis contents .....	5
<b>II LITERATURE REVIEW .....</b>	<b>7</b>
2.1 Introduction.....	7
2.2 Deformation and strength of rocks.....	7
2.3 True triaxial load frame .....	9
2.4 Effect of intermediate principal stresses.....	13
<b>III POLY AXIAL LOAD FRAME .....</b>	<b>16</b>
3.1 Introduction.....	16
3.2 Design requirements and components.....	16
3.3 Calculations of factor of safety.....	19
3.3.1 Calculation of factor of safety of cantilever beam.....	19
3.3.2 Factor of safety of lower beam.....	30
3.3.3 Factor of safety of rectangular column .....	30
3.3.4 Factor of safety of hinge .....	31
3.3.5 Factor of safety of U-link and steel rod .....	31
3.3.6 Factor of safety at screw of rectangular column.....	32
<b>IV LABORATORY TESTING.....</b>	<b>33</b>
4.1 Introduction.....	33
4.2 Sample preparation.....	33
4.3 Characterization tests .....	35

## TABLE OF CONTENTS (Continued)

	<b>Page</b>
4.3.1 Uniaxial compression tests.....	35
4.3.2 Conventional triaxial compression tests.....	35
4.4 True triaxial compression tests .....	39
4.4.1 Test method.....	44
4.4.2 Test results.....	45
4.5 Comparisons .....	46
<b>V DISCUSSIONS, CONCLUSIONS AND RECOMMENDATIONS FOR FUTURE STUDIES.....</b>	<b>64</b>
5.1 Discussions and conclusions .....	64
5.2 Recommendations for future studies.....	65
REFERENCES .....	66
APPENDIX	
APPENDIX A LIST OF PUBLICATIONS .....	69
BIOGRAPHY .....	92

## LIST OF TABLES

Table	Page
4.1 Peak and residual shear strengths for various shear rates of PW sandstone.....	20
4.2 Peak and residual shear strengths for various shear rates of PP sandstone .....	21
4.3 Peak and residual shear strengths for various shear rates of PK sandstone.....	22
4.4 Cohesion and friction angle for various shear rates of PW sandstone.....	24
4.5 Cohesion and friction angle for various shear rates of PP sandstone.....	24
4.6 Cohesion and friction angle for various shear rates of PK sandstone.....	25
4.7 Summary of basic friction angle ( $\phi_b$ ) and cohesion (c).....	28
5.1 Summary of the basic mechanical properties .....	33
5.2 Summary of the factors of safety from computer simulations.....	39

## LIST OF FIGURES

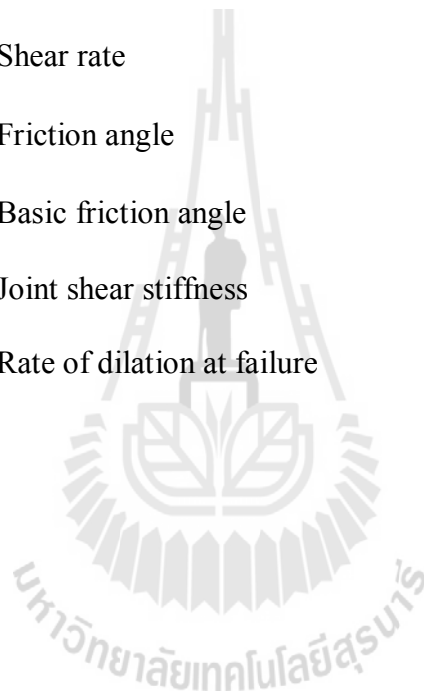
Figure	Page
1.1 Research Methodology.....	3
2.1 Reduction of asperity contact area with progressive shear displacement.....	11
3.1 Some rock specimens prepared for direct shear test.....	14
3.2 A 10×10×16 centimeters block of rock sample is line-loaded to induce tensile fracture in mid-length of the block. ....	15
3.3 Joint roughness coefficient (JRC) of PW, PK and PP sandstone. ....	16
4.1 Direct shear machine (SBEL DR44).....	18
4.2 Pre and post-test PP sandstone specimens .....	18
4.3 Peak (left) and residual (right) shear strengths under various shear rates.....	23
4.4 Cohesion (c) and friction angle ( $\phi$ ) of PW, PP and PK sandstones as a function of the shear rates ( $\delta\tau/\delta t$ ).....	26
4.5 Peak shear strengths of saw cut surface specimens as a function of shear rates .....	27
4.6 Joint shear stiffness as a function of normal stress.....	29
4.7 Parameters $\omega$ and A as a function of shear rate.....	30
5.1 Slope model for computer simulation.....	33
5.2 Computer simulations of PW sandstone by using mechanical properties from shearing rate of $2 \times 10^{-1}$ MPa/s.....	34

## LIST OF FIGURES (Continued)

<b>Figure</b>	<b>Page</b>
5.3 Computer simulations of PW sandstone by using mechanical properties from shearing rate of $2 \times 10^{-5}$ MPa/s .....	34
5.4 Computer simulation of PW sandstone by using mechanical properties of residual strength .....	35
5.5 Computer simulations of PK sandstone by using mechanical properties from shearing rate of $2 \times 10^{-1}$ MPa/s .....	35
5.6 Computer simulations of PK sandstone by using mechanical properties from shearing rate of $2 \times 10^{-5}$ MPa/s .....	36
5.7 Computer simulation of PK sandstone by using mechanical properties of residual strength .....	36
5.8 Computer simulations of PP sandstone by using mechanical properties from shearing rate of $2 \times 10^{-1}$ MPa/s .....	37
5.9 Computer simulations of PP sandstone by using mechanical properties from shearing rate of $2 \times 10^{-5}$ MPa/s .....	38
5.10 Computer simulation of PP sandstone by using mechanical properties of residual strength .....	38

**LIST OF SYMBOLS AND ABBREVIATIONS**

$c$	=	Cohesion
$\sigma_n$	=	Normal stress
$\tau$	=	Shear stress
$\tau_{\text{peak}}$	=	Peak shear stress
$\tau_{\text{residual}}$	=	Residual shear stress
$\delta\tau/\delta t$	=	Shear rate
$\phi$	=	Friction angle
$\phi_b, \phi_\mu$	=	Basic friction angle
$K_s$	=	Joint shear stiffness
$\dot{v}$	=	Rate of dilation at failure



# CHAPTER I

## INTRODUCTION

### 1.1 Background of problems and significance of the study

Joint shear strength is one of the key properties used in the stability analysis and design of engineering structures in rock mass, e.g. slopes, tunnels and foundations. The conventional method currently used to determine the joint shear strength is the direct shear testing which can be performed in the laboratory. In jointed rock masses, joint surface properties such as roughness, separation and joint aperture have considerable effects on shear strength of rock joints. Shear displacements due to earthquake loadings can also affect these parameters. Small repetitive earthquakes cannot make considerable movement, but because of their repetitive nature they may affect the shear resistance of rock joints (Jafari et al., 2002). This also involves the velocity and rate of the shear displacement. Knowledge and understanding of the shear rate on the joint shear strength and stiffness are extremely rare.

### 1.2 Research objectives

The objective of this study is to determine the effects of shear rate on the fracture shear strengths of sandstones. The tested rocks are Phra Wihan, Phu Phan and Phu Kradung sandstones. The fractures are made in the laboratory by tension inducing method. Mathematical relationship between the joint shear strength, loading rate, joint shear stiffness and normal stiffness will be derived. The results will be

applicable to the analysis and design of engineering structures in rock mass where the joint shear strengths may be affected by loading rate induced by seismic, excavation and mining activities.

### **1.3 Research methodology**

The research methodology shown in Figure 1.1 comprises 7 steps; including literature review, sample preparation, direct shear testing, determination of shear stiffness, friction angle and cohesion, development of mathematical relations, conclusions and thesis writing.

#### **1.3.1 Literature Review**

Literature review will be carried out to study the previous researches on joint shear strengths under various shear rates. The sources of information are from text books, journals, technical reports and conference papers. A summary of the literature review will be given in the thesis.

#### **1.3.2 Sample Preparation**

Sample preparation will be carried out in the laboratory at the Suranaree University of Technology. Samples for the direct shear test are prepared to have fractures area of about  $10 \times 10 \text{ cm}^2$ . The fractures will be artificially made in the laboratory by tension inducing method. The joint roughness coefficient (JRC) for each fracture will be determined. A total of 15 samples will be prepared for each shear rate.

#### **1.3.3 Direct Shear Testing**

The test method follows the ASTM (D5607-08) standard practice. The constant normal stresses on the fracture are 0.2, 1, 2, 3 and 4 MPa. The test is



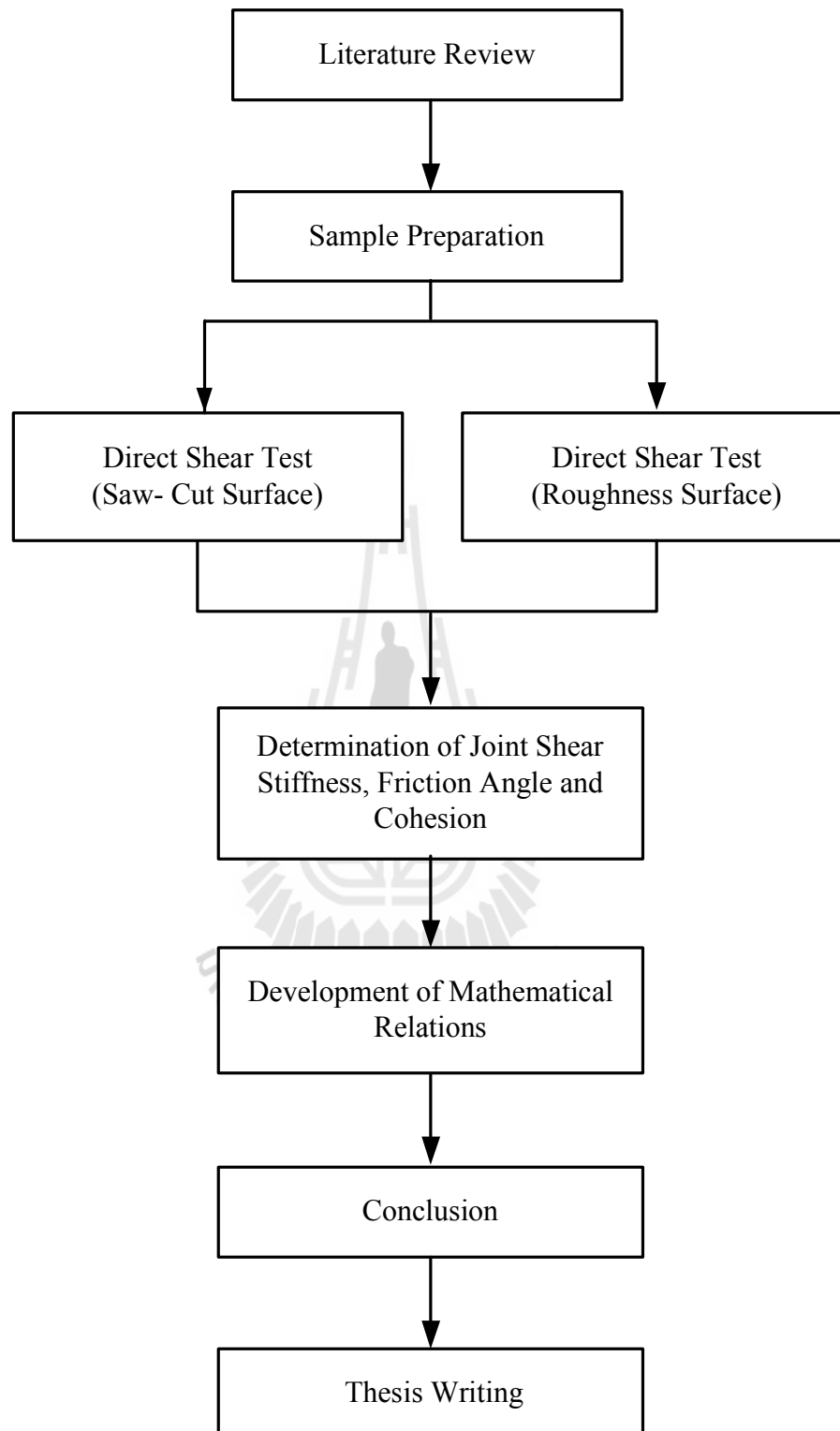


**Figure 1.1** Research Methodology

terminated when a total of 8 mm of shear displacement is reached. The shear rates vary from  $2 \times 10^{-5}$  to  $2 \times 10^{-1}$  MPa/s.

#### **1.3.4 Determination of Joint Shear Stiffness, Friction Angle and Cohesion**

Test results will be used to determine the joint shear stiffness from shear stress and displacement curves. The friction angle and cohesion will be determined from the normal and shear stress relations at the peak and residual regions.

#### **1.3.5 Development of Mathematical Relations**

Results from laboratory test will be used to formulate mathematical relations between the joint shear strengths, loading rates, joint shear stiffness and normal stress.

#### **1.3.6 Conclusions**

All research activities, methods, and results will be documented and compiled in the thesis. The research or findings will be published in the conference proceedings or journals.

#### **1.3.7 Thesis Writing**

All research activities, methods, and results will be documented and compiled in the thesis. The research or findings will be published in the journals.

### **1.4 Scope and limitations of the study**

The scope and limitations of the research include as follows.

1. Laboratory testing will be conducted on sandstone specimens from Phra Wihan, Phu Kradung and Phu Phan sandstones.
2. The applied normal stresses ( $\sigma_n$ ) vary from 0.2, 1, 2, 3 to 4 MPa.

3. The applied shearing rates ( $\delta\tau/\delta t$ ) vary from  $2\times 10^{-5}$  to  $2\times 10^{-1}$  MPa/s.
4. Up to 25 samples will be tested, with the nominal sample sizes of  $10\times 10\times 16$  cm<sup>3</sup>.
5. Testing will be made under dry condition.
6. All tests will be conducted under ambient temperature.

## 1.5 Thesis contents

**Chapter I** introduces the thesis by briefly describing the background of problems and significance of the study. The research objectives, methodology, scope and limitations are identified. **Chapter II** summarizes results of the literature review. **Chapter III** describes the sample preparation and laboratory experiment. **Chapter IV** presents the results obtained from the laboratory testing. **Chapter V** describes the numerical modeling to predict the stability of slope by FLAC. **Chapter VI** concludes the research results, and provides recommendations for future research studies. **Appendix A** provides detailed result of direct shear testing.

## CHAPTER II

### LITERATURE REVIEW

#### 2.1 Introduction

This chapter summarizes the results of literature review carried out to improve an understanding of loading rate effects on joint shear strength.

#### 2.2 Effect of Loading Rate

Frictional resistance of rock joints is dependent of the rate of shear displacement. The magnitude of this effect is quite variable, depending mainly on the rock type and normal stress level. In general, for harder rocks, the frictional resistance has been found to decrease with increasing shear displacement rates greater than a variable critical velocity (Crawford and Curran, 1981).

Vasarhelyi (1998) has studied the influence of normal load on joint dilatation rate. The results show that the measured dilatation angle decreases with the increased normal force and it is always present. However, the Equation 2.1 is also correct for the cases when the Patton and the Seidel and Haberfield equations fail.

$$\tau = \sigma_n \tan (\phi_\mu + \dot{V}) \quad (2.1)$$

where  $\phi_\mu$  = basic friction angle and  $\dot{V}$  = the rate of dilation at failure.

This means that this is a more general equation and it should be valid until the “teeth” (or irregularities) are not shorn off. This point is not at the transition stress,

rather the meeting point of the Jaeger curve and the bilinear curve. The measured dilatation-displacement curves show that, after the peak stress, the rate of dilatation does not change until a lot later.

Jafari et al. (2003) have studied the effects of displacement rates (or shearing velocity) on shear strength, some monotonic tests were performed in different ranges of axial displacement in 4 MPa confining pressure from 0.05 to 0.4 mm/s. The differences between the curves can be related to the effects of shear velocity on second-order asperities, as the total applied displacement is limited. It is observed that shear strength reduces with increasing shear velocity, approaching the same values for the peak and residual strength at higher shearing velocities.

Park and Song (2009) perform direct shear test on a rock joint using a bonded-particle model. The normal stresses applied to the sample were 3 and 15 MPa, which are approximately 2% and 10% of the uniaxial strength of the intact sample, respectively. The shear stress increase rapidly until the peak strength was passed, and reached some residual value that remained constant as the displacement continued. The peak and residual strengths were 5.33 and 1.82 MPa at low normal stress and 15.5 and 5.77 MPa at high normal stress. The friction calculated from the ratio of the peak shear strength to the given normal stress was higher at lower normal stress: 1.78 at 3 MPa and 1.03 at 15 MPa. The rate of change in normal displacement showed a maximum value at the peak shear stress level and decreased gradually in both cases. The normal displacement continued to increase at low normal stress, while it converged at high normal stress when the residual state reached. The normal displacements at a shear displacement of 1.6 mm were 0.795 mm at 3 MPa and 0.434 mm at 15 MPa. These are approximately 2.21% and 1.21% of the sample height of 36 mm, respectively. There were a larger number of normal cracks (tensile cracks)

than the shear cracks, and the total number increased with increasing normal stress: 650 cracks at 3 MPa and 3290 at 15 MPa. For reference, the number of joint contacts was 5,196 at the initial stage. The cracks were initiated at 80% of the peak (pre-peak), and propagated rapidly until the shear stress reached 80% of the peak stress after passing the peak (post-peak). After the first crack was initiated, the shear stress showed a non-linear relationship with the shear displacement.

### **2.3 Effect of Joint Roughness**

Kwafniewski and Wang (1997) have studied the surface roughness evolution and mechanical behavior of rock joints under shear. The shear behavior of rock joints characterized by the shear stiffness and peak shear strength depends mainly on the normal load applied. The shear stiffness and shear strength have relatively smaller values. Experiments show a complex dependence of shear stiffness and the peak shear strength on the roughness. The shear behavior of rock joints characterized by the shear stiffness and peak shear strength depends mainly on the normal load applied. Experimental results show that, at a lower  $\theta$ , the shear stiffness and shear strength have relatively smaller values. In such a case, the shear resistance drops once the peak shear strength has been achieved. At a higher  $\theta$ , however, both shear stiffness and the peak shear strength significantly increase and the drop in shear resistance after the peak shear strength becomes more evident. For  $\theta = 45^\circ$ , i. e. high normal force conditions, a number of significant peaks have been normally recorded in the post-initial yield region. When subjected to normal and tangential loads, the rough surfaces of rock joints experience damage in the process of shearing. The failure mode of asperities on the joint surfaces and the degradation of surface structure depend on the normal force applied as well as the shear history. The physical process

of surface damage is in fact considerably complex. Due to the random character of surface structure, it is quite possible that the damage of a rough surface occurs as a result of several mechanisms. For instance, tensile split occurs at steeper asperities in one part, while sliding or rotation of failed asperities in another part of the joint. Moreover, in some sequences, individual mechanisms of surface damage may take place in the loading history. The observed macrochanges in the surface topography actually tell only a part of the story of the damage process.

Lee et al. (2001) proposed a cyclic shear testing system that was established to investigate the mechanical behavior of rough rock joints under cyclic loading conditions. Laboratory cyclic shear tests were conducted for two joint types of Hwangdeung granite and Yeosan marble, saw-cut and split tensile joints. Prior to the test, the roughness of each specimen was characterized by measuring the surface topography using a laser profilometer. Monotonic shear behaviors of rough joints were simulated using the proposed model in this study. Input parameters were obtained based on the results of laboratory tests. Initial asperity angles and damage coefficients were also calculated from the results of laser profilometer analysis and asperity degradations. Simulated shear behaviors of three rough joint specimens are superimposed on the laboratory test results. The proposed model precisely simulated the peak shear stresses and the shear stress–shear displacement relations from numerical simulations were closely matched with the laboratory test results. Simulated dilation curves could also replicate the general trend of nonlinear changes for rough joint as discovered in the experimental results.

Seidel and Haberfield (2002) investigated the behaviour of rock joints subjected to direct shear. Both concrete/rock and rock/rock joints were investigated. The behaviour of rock/rock joints is important for the assessment of stability issues

involving rock masses (e.g. rock slope stability). Concrete/rock joints are vital to the assessment of performance of concrete piles socketed into rock, rock anchors and concrete dam foundations. Initially, before the commencement of sliding, the two halves of the joint are assumed to be in intimate contact with both faces of each asperity in full contact. After the initiation of interface slip, the contact area between the two halves of the joint is restricted to one asperity face, and progressively reduces as shear displacement progresses. This is demonstrated in Figure 2.1 for an interface comprising regular triangular asperities. Local normal stresses increase both as a consequence of the reduced contact area and as a result of the increasing normal stress due to the constant normal stiffness (CNS) condition. A critical normal stress is reached at which the asperity can no longer sustain the loading and individual asperity failure results. The asperity shearing mechanism was observed to differ between Johnstone/Johnstone (J/J) and Johnstone/Concrete (J/C) joints. For J/C joints, the much stronger half of the joint constrained failure over the full contact length of each asperity. However, for J/J joints the material on both sides of the interface is similar, allowing failure to occur at localized regions of high stress that occur at the leading and trailing points of contact of each asperity. Failure gradually progressed from these localized regions until complete failure of each asperity (and therefore of the whole interface) occurred. This resulted in a significant reduction in the measured strength. The finite difference program FLAC was used to investigate the failure of both J/J and J/C interfaces. The results of this analysis indicated that the ultimate failure mode in J/J joints was similar to that of J/C joints, but failure occurred at a lower stress. A stress reduction factor of 1.38 was found to be appropriate for J/J joints.



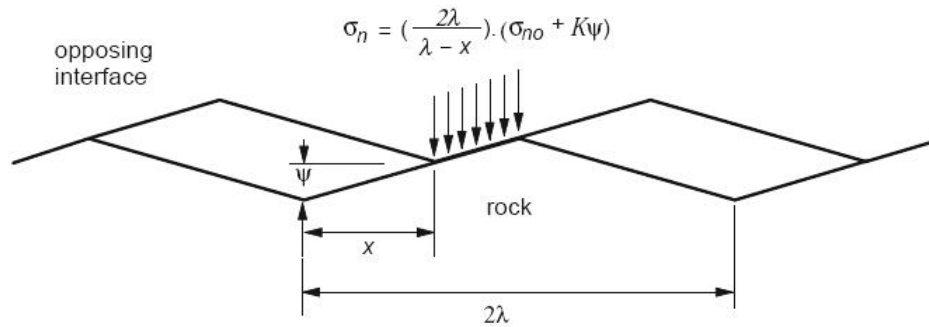


**Figure 2.1.** Reduction of asperity contact area with progressive shear displacement (Seidel and Haberfield, 2002).

Kemeny (2003) developed a fracture mechanics model to illustrate the importance of time dependence for brittle fractured rock. In particular a model is developed for the time dependent degradation of rock joint cohesion. Degradation of joint cohesion is modeled as the time-dependent breaking of intact patches or rock bridges along the joint surface. A fracture mechanics model is developed utilizing subcritical crack growth, which results in a closed-form solution for joint cohesion as a function of time. As an example, a rock block containing rock bridges subjected to plane sliding is analyzed. The cohesion is found to continually decrease, at first slowly and then more rapidly. At a particular value of time the cohesion reduces to value that result in slope instability. A second example is given where variations in some of the material parameters are assumed. A probabilistic slope analysis is conducted, and the probability of failure as a function of time is predicted. The probability of failure is found to increase with time, from an initial value of 5% to a value at 100 years of over 40%. These examples show the importance of being able to predict the time dependent behavior of a rock mass containing discontinuities, even for relatively short-term rock structures.

Kemthong and Fuenkajorn (2007) perform direct shear test on saw-cut specimens to determine the relationship between the basic friction angle ( $\phi_b$ ) and the rock compressive strength (UCS). Testing on specimens with tension-induced fractures yielded joint shear strengths under different JRC's for use in the verification. The results indicate that Barton's criterion using the field-identified parameters can satisfactorily predict the shear strengths of rough joints in marble and sandstones, and slightly over-predicts the shear strength in the basalt specimens. It cannot however describe the joint shear strengths for the granite specimens. This is probably because the saw-cut surfaces for coarse-grained and strong crystalline rocks are very smooth resulting in an unrealistically low  $\phi_b$ . Barton's shear strength criterion is more sensitive to  $\phi_b$  than to UCS and JRC. For all sandstones the  $\phi_b$  values are averaged as  $33 \pm 8$  degrees, apparently depending on their cementing materials. The average  $\phi_b$  for the tested marbles and for the limestone recorded elsewhere  $35 \pm 3$  degrees, and is independent of UCS. The  $\phi_b$  values for other rock types apparently increase with UCS particularly for very strong rocks. The factors governing  $\phi_b$  for crystalline rocks are probably crystal size, mineral compositions, and the cutting process, and for clastic rocks are grain size and shape and the strength of cementing materials.

## **CHAPTER III**

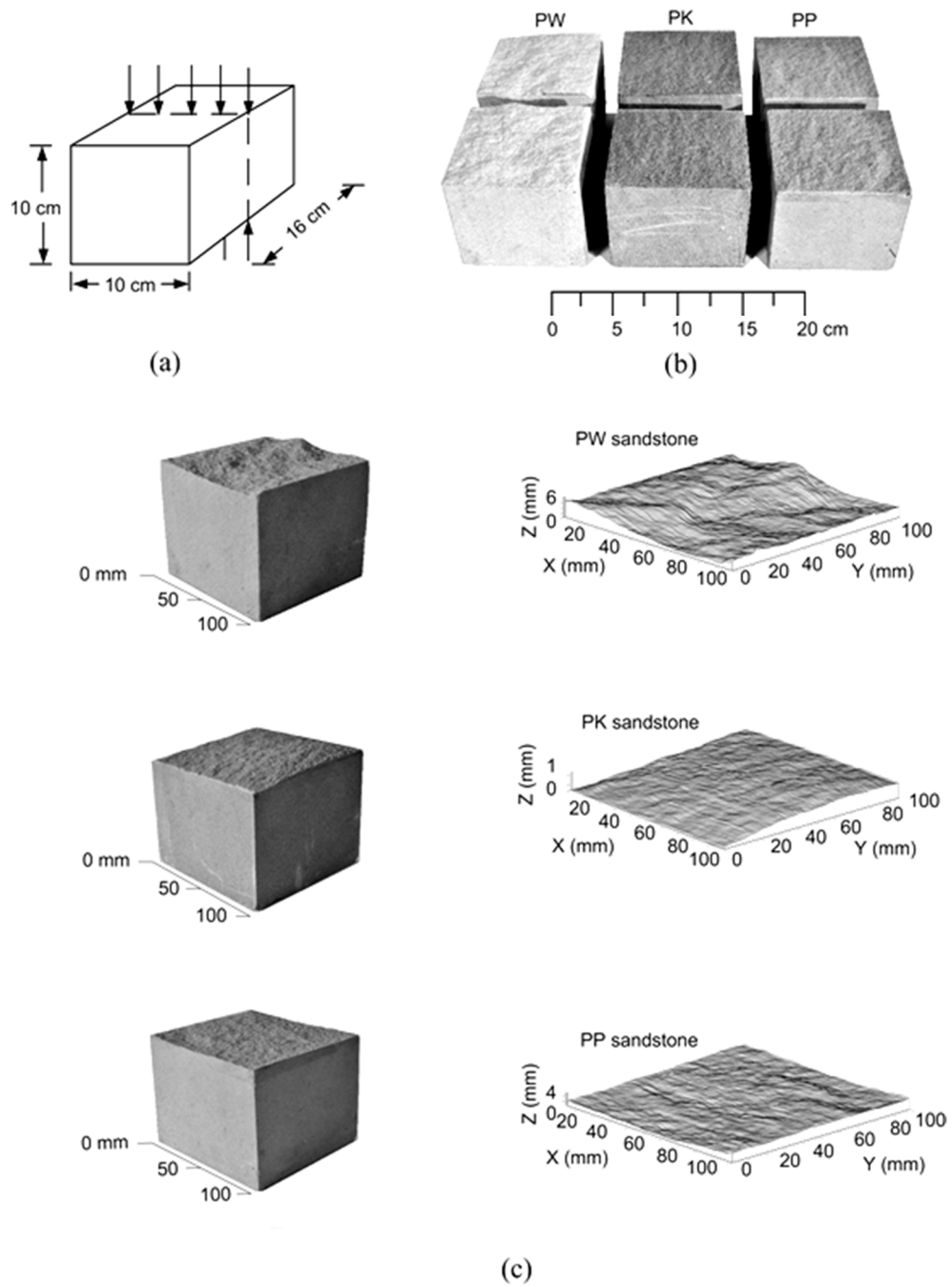
### **SAMPLE PREPARATION**

#### **3.1 Introduction**

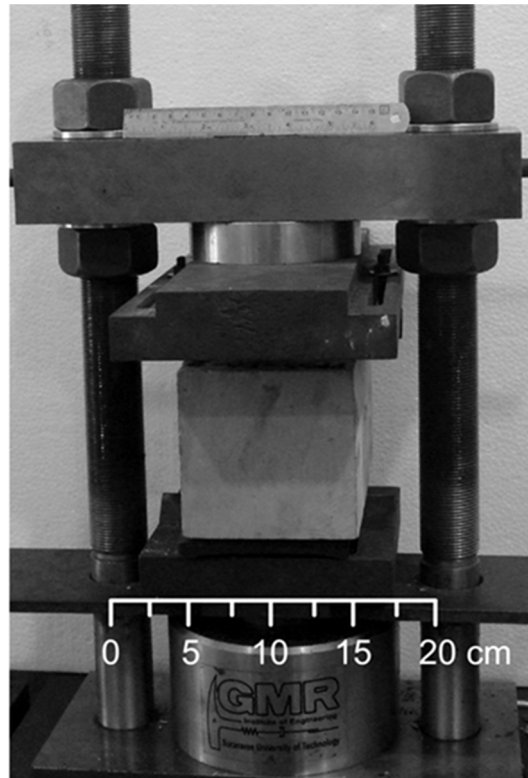
This chapter describes the rock sample preparation. The rock samples include Pra Wihan, Phu Kradung and Phu Phan sandstone (hereafter designated as PW, PK and PP sandstones) (Figure 3.1). These rocks have significant impacts on stability of many engineering structures constructed in region (slope embankments, underground mines and tunnels). They are selected here due to their uniform texture and availability.

#### **3.2 Sample preparation**

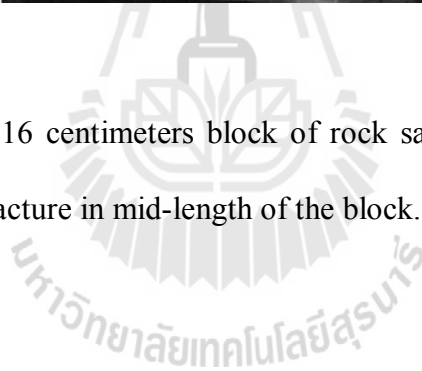
A minimum of 25 specimens are prepared for each rock type. The sample preparation is carried out in the laboratory at the Suranaree University of Technology. Specimens for the direct shear test are prepared to have fractures area of about 10×10 square centimeters. The fractures are artificially made in the laboratory by tension inducing and saw cut methods in 10×10×16 cm<sup>3</sup> prismatic blocks of rocks samples (Figure 3.2). These rocks are classified as fine-grained quartz sandstones with highly uniform texture and density. Their roughness is observed and classified by comparing with a reference profiles given by Barton (joint roughness coefficient-JRC, Barton, 1973). For all sandstone specimens the joint roughness coefficients of the tension-induced fractures are in the range between 6 and 12. Figure 3.3 shows the joint roughness of rock samples.



**Figure 3.1** Some rock specimens prepared for direct shear test.



**Figure 3.2** A 10×10×16 centimeters block of rock sample is line-loaded to induce tensile fracture in mid-length of the block.



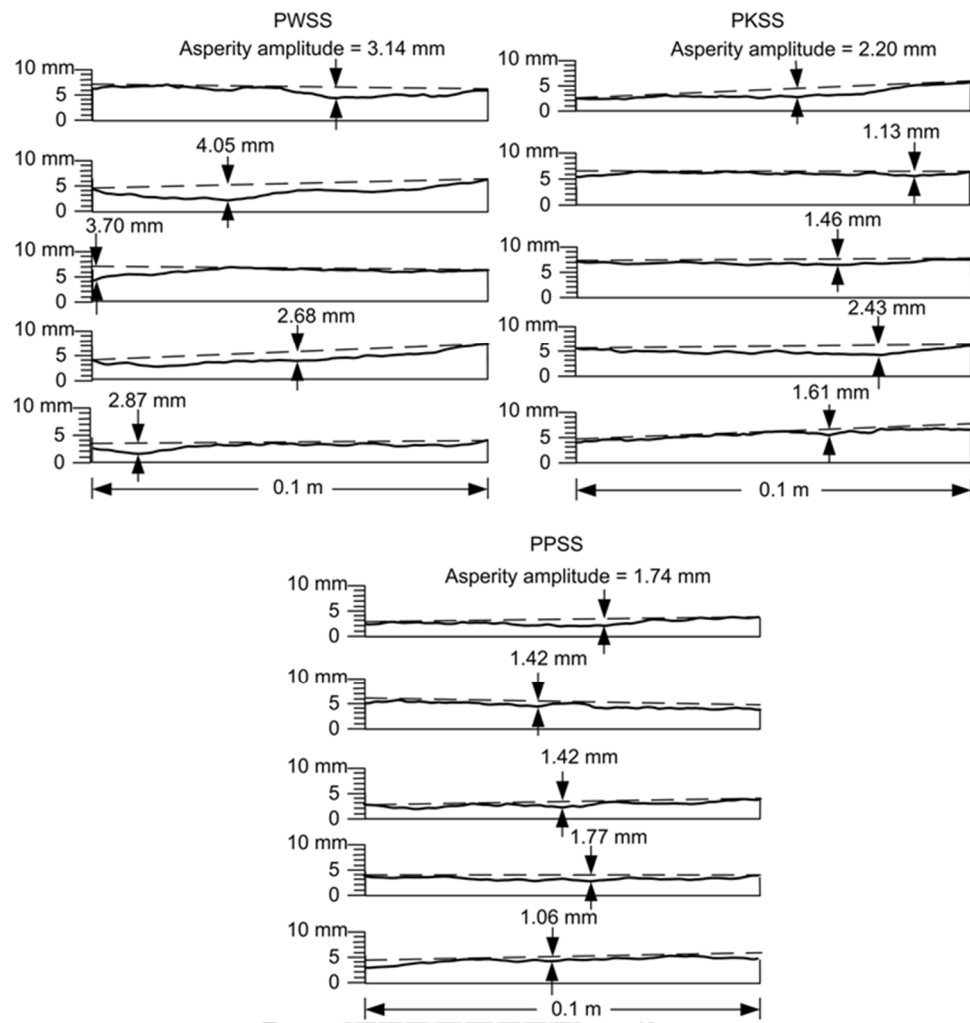


**Figure 3.3** Joint roughness coefficient (JRC) of PW, PK and PP. (JRC = 12, 7 and 6)

## **CHAPTER IV**

### **LABORATORY TESTING**

#### **4.1 Introduction**

The objective of the laboratory testing is to assess the effects of shear rate on fracture shear strengths by performing series of direct shear testing on tension-induced fractures and smooth saw-cut surfaces in sandstone specimens. Mathematical relations are proposed to empirically determine the joint shear strengths and shear stiffness under various loading rates.

#### **4.2 Test method**

The direct shear tests are performed with the normal stresses of 0.2, 1, 2, 3 and 4 MPa for the rough fractures and of 0.2, 1, 2 and 3 MPa for the smooth surfaces. The test method and calculation follow as much as practical the ASTM (D5607-08) standard practice. Each specimen is sheared only once under the predefined constant normal stress using a direct shear machine (SBEL DR44). Figure 4.1 show the laboratory arrangement of the direct shear test while the fracture is under normal and shear stresses. The shearing rates are 0.00002, 0.0002, 0.002, 0.02 and 0.2 MPa/s. The shear force is continuously applied until a total shear displacement of 8 mm is reached. The applied normal and shear forces and the corresponding normal and shear displacements are monitored and recorded. Post-test observation on the sheared off area indicates that the asperity areas that have been sheared off are small for all specimens, about 10 - 15% of the

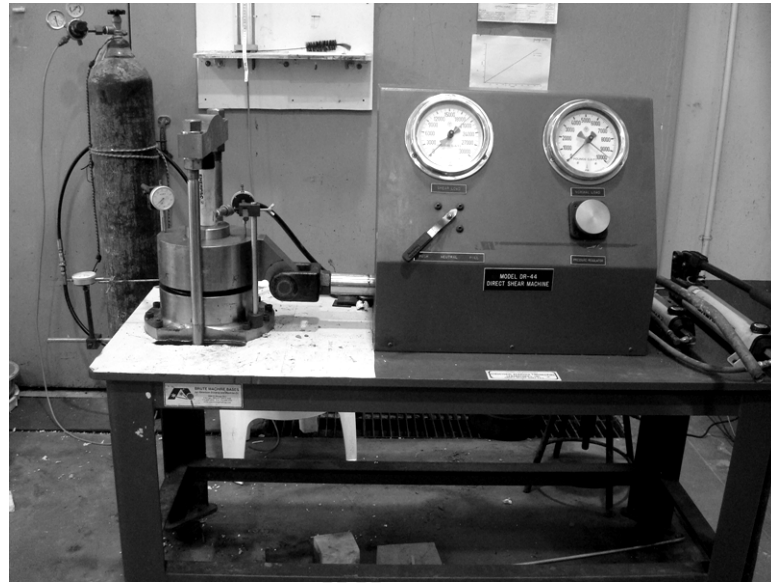


**Figure 4.1** Direct shear machine (SBEL DR44).

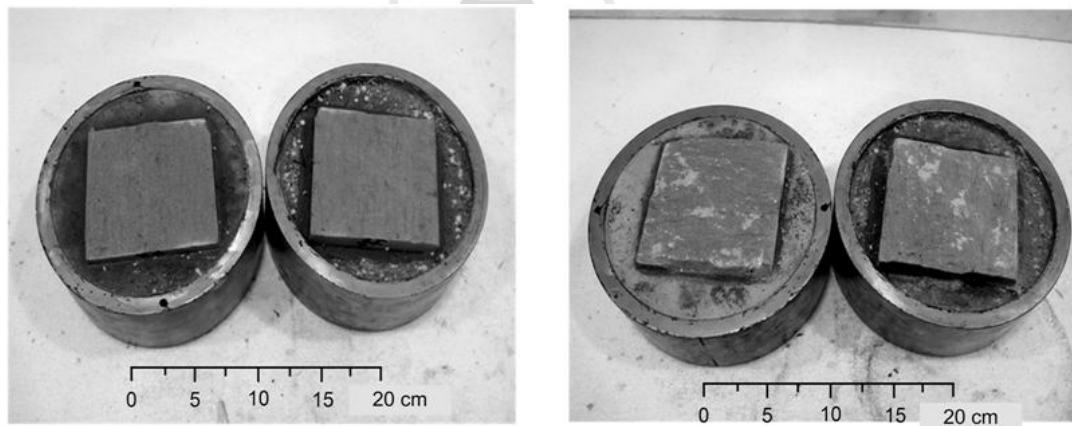


**Figure 4.2** Pre and post-test PP sandstone specimens.

total area. Figure 4.2 shows the pre and post-test fractures for the PP sandstone specimens.



## 4.2 Test results

Tables 4.1 through 4.3 list the peak and residual shear stresses for all specimens. The shear rates are determined by divided the loading rates by the specimen area. Figure 4.3 shows the peak and residual shear stresses of PW, PK and PP sandstones as a function of normal stress for various shear rates ( $\delta\tau/\delta t$ ). The higher the loading rate applied, the higher the peak and residual shear stresses are obtained. According to the Coulomb criterion the shear stress ( $\tau$ ) can be represented by:

$$\tau = c + \sigma_n \tan \phi \quad (4.1)$$

where  $\sigma_n$  is the normal stress,  $c$  is the cohesion and  $\phi$  is the friction angle. The cohesion and friction angle of all specimens are summarized in Table 4.4 to table 4.6. They can be determined as a function of the shear rate as follows (Figure 4.4):

$$c = X \cdot \ln(\delta\tau/\delta t) + Y \quad (4.2)$$

$$\phi = Z \cdot \ln(\delta\tau/\delta t) + B \quad (4.3)$$

Substituting equations (4.2) and (4.3) into (4.1) the shear stress ( $\tau$ ) can be written as:

$$\tau = [ X \cdot \ln(\delta\tau/\delta t) + Y ] + \sigma_n \tan [ Z \cdot \ln(\delta\tau/\delta t) + B ] \quad (4.4)$$

**Table 4.1** Peak and residual shear strengths for various shear rates of PW sandstone.

$\sigma_n$ (MPa)	$\delta\tau/\delta t$ (MPa/s)	PW sandstone	
		$\tau_{\text{peak}}$ (MPa)	$\tau_{\text{residual}}$ (MPa)
0.2	$2 \times 10^{-1}$	0.69	0.46
	$2 \times 10^{-2}$	0.45	0.30
	$2 \times 10^{-3}$	0.42	0.24
	$2 \times 10^{-4}$	0.29	0.18
	$2 \times 10^{-5}$	0.19	0.17
1	$2 \times 10^{-1}$	1.90	1.23
	$2 \times 10^{-2}$	1.63	1.04
	$2 \times 10^{-3}$	1.43	0.80
	$2 \times 10^{-4}$	1.08	0.72
	$2 \times 10^{-5}$	1.04	0.63
2	$2 \times 10^{-1}$	3.16	2.60
	$2 \times 10^{-2}$	3.01	2.44
	$2 \times 10^{-3}$	2.62	2.07
	$2 \times 10^{-4}$	2.53	1.89
	$2 \times 10^{-5}$	2.17	1.71
3	$2 \times 10^{-1}$	4.21	3.73
	$2 \times 10^{-2}$	4.06	3.47
	$2 \times 10^{-3}$	3.78	3.07
	$2 \times 10^{-4}$	3.62	2.54
	$2 \times 10^{-5}$	3.23	2.24
4	$2 \times 10^{-1}$	5.28	4.46
	$2 \times 10^{-2}$	4.95	4.18
	$2 \times 10^{-3}$	4.77	3.99
	$2 \times 10^{-4}$	4.33	3.75
	$2 \times 10^{-5}$	4.06	3.38

**Table 4.2** Peak and residual shear strengths for various shear rates of PP sandstone.

$\sigma_n$ (MPa)	$\delta\tau/\delta t$ (MPa/s)	PP sandstone	
		$\tau_{\text{peak}}$ (MPa)	$\tau_{\text{residual}}$ (MPa)
0.2	$2 \times 10^{-1}$	0.76	0.38
	$2 \times 10^{-2}$	0.49	0.30
	$2 \times 10^{-3}$	0.30	0.26
	$2 \times 10^{-4}$	0.26	0.24
	$2 \times 10^{-5}$	0.22	0.22
1	$2 \times 10^{-1}$	1.87	1.25
	$2 \times 10^{-2}$	1.64	1.06
	$2 \times 10^{-3}$	1.29	0.99
	$2 \times 10^{-4}$	1.12	0.95
	$2 \times 10^{-5}$	0.99	0.82
2	$2 \times 10^{-1}$	3.02	2.50
	$2 \times 10^{-2}$	2.79	2.38
	$2 \times 10^{-3}$	2.60	2.17
	$2 \times 10^{-4}$	2.22	1.97
	$2 \times 10^{-5}$	2.00	1.72
3	$2 \times 10^{-1}$	4.48	3.45
	$2 \times 10^{-2}$	4.14	3.28
	$2 \times 10^{-3}$	3.49	2.80
	$2 \times 10^{-4}$	2.97	2.32
	$2 \times 10^{-5}$	2.76	2.24
4	$2 \times 10^{-1}$	5.79	4.45
	$2 \times 10^{-2}$	5.17	4.22
	$2 \times 10^{-3}$	4.54	3.83
	$2 \times 10^{-4}$	4.19	3.65
	$2 \times 10^{-5}$	4.03	3.26

**Table 4.3** Peak and residual shear strengths for various shear rates of PK sandstone.

$\sigma_n$ (MPa)	$\delta\tau/\delta t$ (MPa/s)	PK sandstone	
		$\tau_{\text{peak}}$ (MPa)	$\tau_{\text{residual}}$ (MPa)
0.2	$2 \times 10^{-1}$	0.56	0.33
	$2 \times 10^{-2}$	0.37	0.25
	$2 \times 10^{-3}$	0.29	0.17
	$2 \times 10^{-4}$	0.17	0.14
	$2 \times 10^{-5}$	0.17	0.14
1	$2 \times 10^{-1}$	1.48	0.98
	$2 \times 10^{-2}$	1.28	0.96
	$2 \times 10^{-3}$	1.15	0.91
	$2 \times 10^{-4}$	0.94	0.81
	$2 \times 10^{-5}$	0.76	0.58
2	$2 \times 10^{-1}$	2.67	1.97
	$2 \times 10^{-2}$	2.53	1.72
	$2 \times 10^{-3}$	2.13	1.54
	$2 \times 10^{-4}$	1.79	1.34
	$2 \times 10^{-5}$	1.60	1.26
3	$2 \times 10^{-1}$	3.62	2.68
	$2 \times 10^{-2}$	3.23	2.45
	$2 \times 10^{-3}$	2.97	2.28
	$2 \times 10^{-4}$	2.71	2.12
	$2 \times 10^{-5}$	2.43	2.07
4	$2 \times 10^{-1}$	4.38	3.11
	$2 \times 10^{-2}$	4.19	2.99
	$2 \times 10^{-3}$	3.80	2.71
	$2 \times 10^{-4}$	3.44	2.48
	$2 \times 10^{-5}$	3.22	2.34

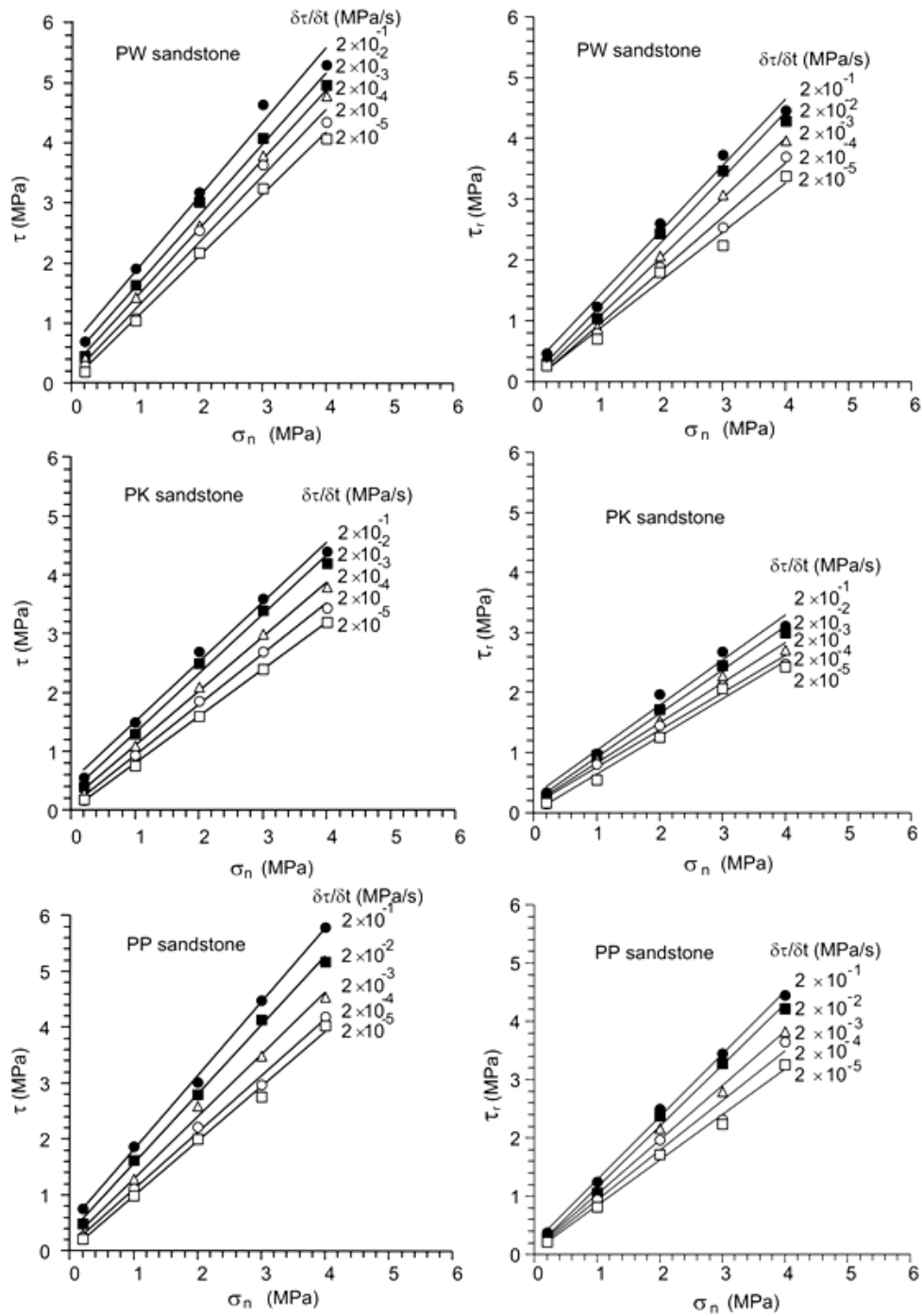


Figure 4.3 Peak (left) and residual (right) shear strengths under various shear rates.

**Table 4.4** Cohesion and friction angle for various shear rates of PW sandstone.

Shear stress	$\delta\tau/\delta t$ (MPa/s)	PW sandstone		
		c (MPa)	$\phi$ (Degrees)	R <sup>2</sup>
$\tau_{\text{peak}}$	$2 \times 10^{-1}$	0.61	51.0	0.99
	$2 \times 10^{-2}$	0.40	49.9	0.99
	$2 \times 10^{-3}$	0.26	49.0	0.99
	$2 \times 10^{-4}$	0.12	47.9	0.99
	$2 \times 10^{-5}$	0.03	45.9	0.99
$\tau_{\text{residual}}$	$2 \times 10^{-1}$	0.27	47.5	0.99
	$2 \times 10^{-2}$	0.09	47.3	0.99
	$2 \times 10^{-3}$	0.03	44.9	0.99
	$2 \times 10^{-4}$	0.01	41.9	0.99
	$2 \times 10^{-5}$	0.02	39.1	0.98

**Table 4.5** Cohesion and friction angle for various shear rates of PP sandstone.

Shear stress	$\delta\tau/\delta t$ (MPa/s)	PP sandstone		
		c (MPa)	$\phi$ (Degrees)	R <sup>2</sup>
$\tau_{\text{peak}}$	$2 \times 10^{-1}$	0.49	52.8	0.99
	$2 \times 10^{-2}$	0.33	51.0	0.99
	$2 \times 10^{-3}$	0.18	47.9	0.99
	$2 \times 10^{-4}$	0.09	45.3	0.99
	$2 \times 10^{-5}$	0.002	44.1	0.99
$\tau_{\text{residual}}$	$2 \times 10^{-1}$	0.30	47.1	0.99
	$2 \times 10^{-2}$	0.20	46.3	0.99
	$2 \times 10^{-3}$	0.11	43.0	0.99
	$2 \times 10^{-4}$	0.07	40.5	0.98
	$2 \times 10^{-5}$	0.001	38.0	0.99

**Table 4.6** Cohesion and friction angle for various shear rates of PK sandstone.

Shear stress	$\delta\tau/\delta t$ (MPa/s)	PK sandstone		
		c (MPa)	$\phi$ (Degrees)	R <sup>2</sup>
$\tau_{\text{peak}}$	$2 \times 10^{-1}$	0.48	45.5	0.99
	$2 \times 10^{-2}$	0.30	45.2	0.99
	$2 \times 10^{-3}$	0.17	42.9	0.99
	$2 \times 10^{-4}$	0.10	40.8	0.99
	$2 \times 10^{-5}$	0.006	38.6	0.99
$\tau_{\text{residual}}$	$2 \times 10^{-1}$	0.28	37.0	0.98
	$2 \times 10^{-2}$	0.19	36.0	0.99
	$2 \times 10^{-3}$	0.16	33.8	0.99
	$2 \times 10^{-4}$	0.06	33.5	0.98
	$2 \times 10^{-5}$	0.001	32.1	0.99



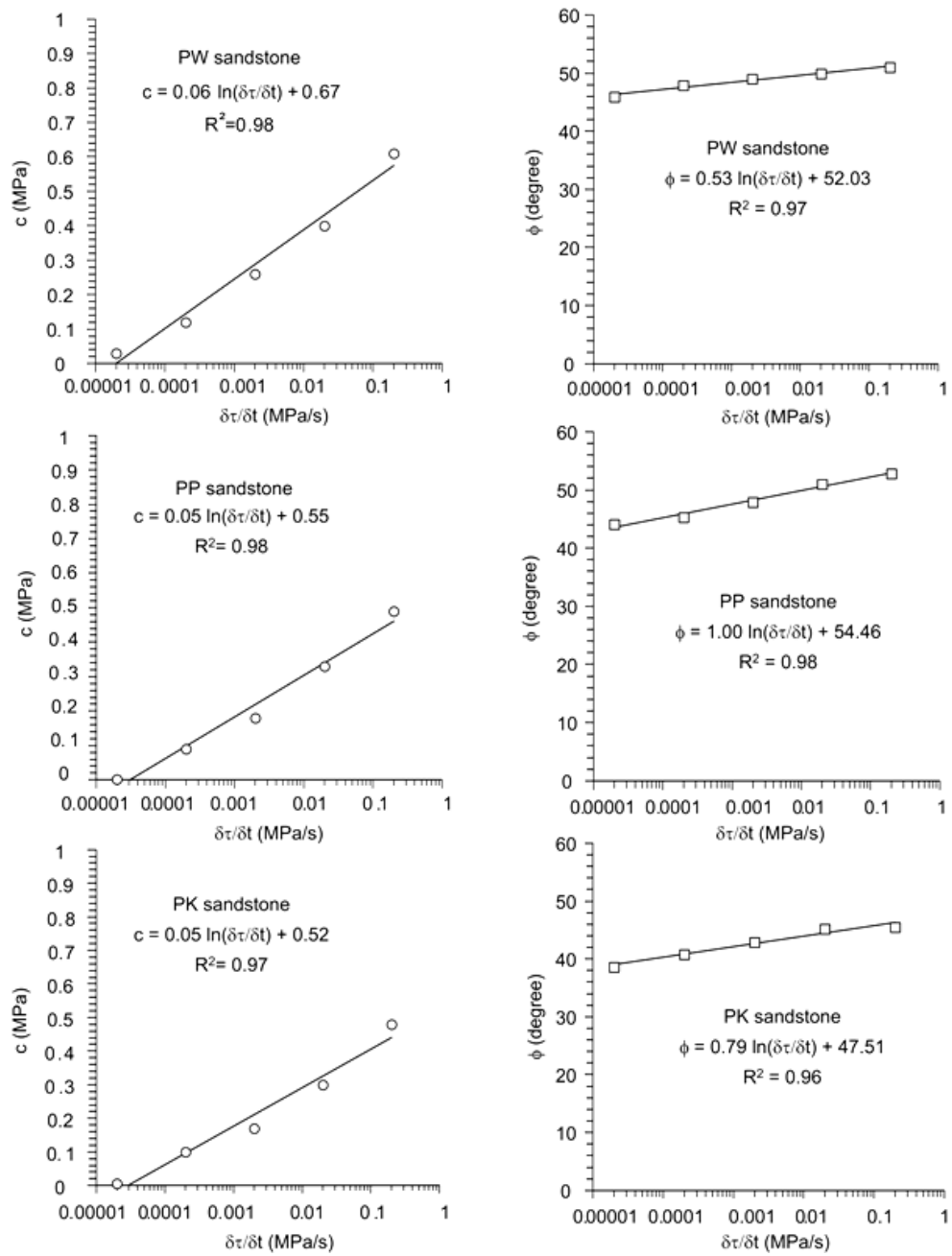


**Figure 4.4** Cohesion ( $c$ ) and friction angle ( $\phi$ ) of PW, PP and PK sandstones as a function of the shear rates ( $\delta\tau/\delta t$ ).



The logarithmic relations used above are suitable for the tested sandstone fractures. They however may not represent the shear behavior of other rock types with different fracture characteristics from those tested here. Figure 4.5 shows the peak shear strengths of the saw cut surfaces. The results clearly show that the strengths of the smooth surface are independent of the shear rate (Table 4.7).

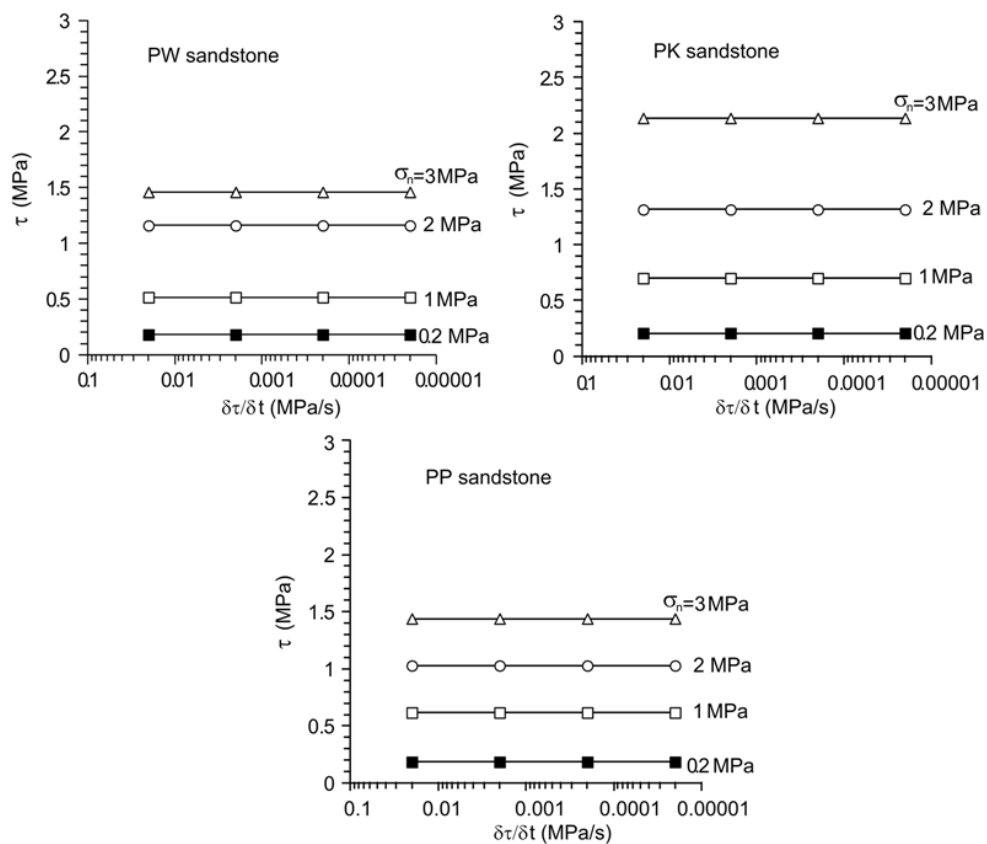


**Figure 4.5** Peak shear strengths of saw cut surface specimens as a function of shear rates.

**Table 4.7** Summary of basic friction angle ( $\phi_b$ ) and cohesion (c).

Rock type	$\phi_b$	c
PW sandstone	25.6	0.09
PP sandstone	23.8	0.13
PK sandstone	34.2	0.03

## 5 Joint shear stiffness

Figure 4.6 plots the joint shear stiffness,  $K_s$  as a function of the normal stress. It is calculated from the linear slope of the shear stress-displacement curves ( $\delta\tau/\delta t$ ). The shear stiffness tends to linearly increase with increasing the normal stress which can be represented by:

$$K_s = \omega \cdot \sigma_n + A \quad (4.5)$$

where  $\omega$  and  $A$  are empirical constants depending on the shear rate applied. Figure 4.7 shows the parameters  $\omega$  and  $A$  of the PW, PK and PP sandstones as a function of the shear rates ( $\delta\tau/\delta t$ ). They can be represented by the following relations:

$$\omega = \alpha \cdot \ln(\delta\tau/\delta t) + L \quad (4.6)$$

$$A = \beta \cdot (\delta\tau/\delta t)^\kappa \quad (4.7)$$

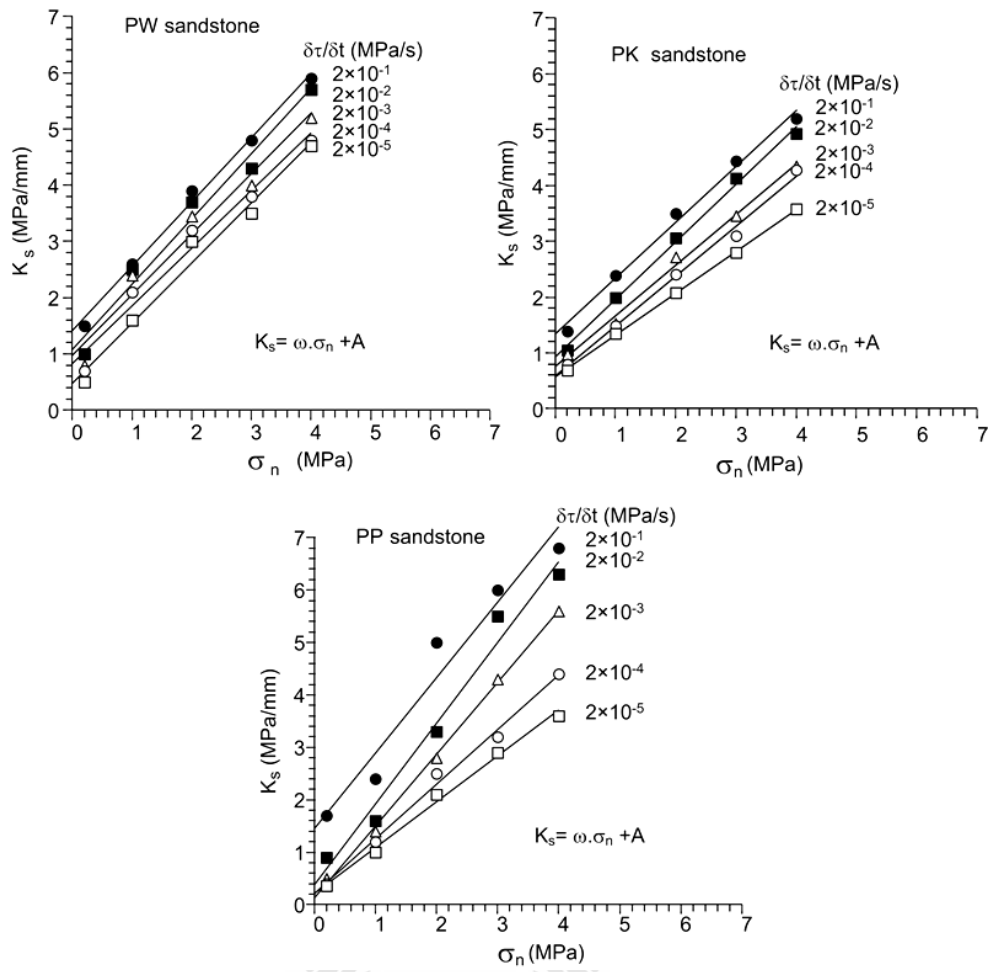
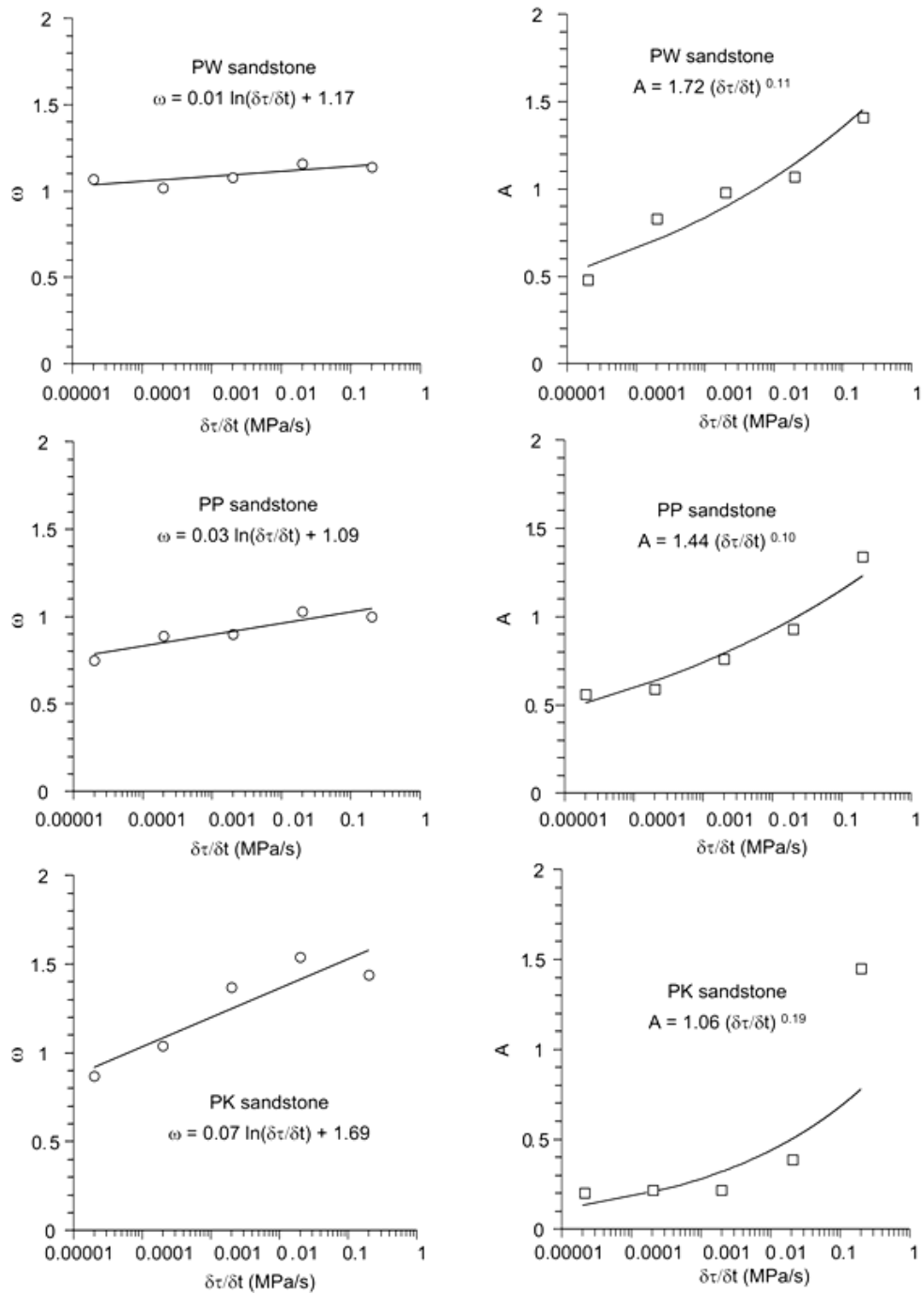


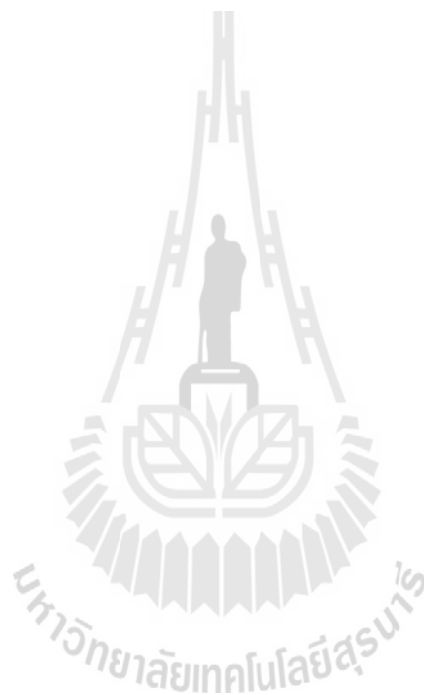
Figure 4.6 Joint shear stiffness as a function of normal stress.



**Figure 4.7** Parameters  $\omega$  and  $A$  as a function of shear rate.

The parameters  $\alpha$ ,  $L$ ,  $\beta$  and  $\kappa$  are empirical constants (Table 4). Substituting equations (4.7) and (4.6) into (4.5) the joint shear stiffness ( $K_s$ ) can be written as:

$$K_s = [\alpha \cdot \ln(\delta\tau/\delta t) + L] \cdot \sigma_n + [\beta \cdot (\delta\tau/\delta t)^\kappa] \quad (4.8)$$



# **CHAPTER V**

## **COMPUTER MODELING**

### **5.1 Introduction**

This chapter describes the stability analysis using FLAC (Itasca, 1994) to study the stability of rock slope due to the low shearing rate of a rock joint on slope. Results from factor of safety (FS) analysis are used in the evaluation of the stability as affected by the various shearing rate.

### **5.2 Rock properties for computer modeling**

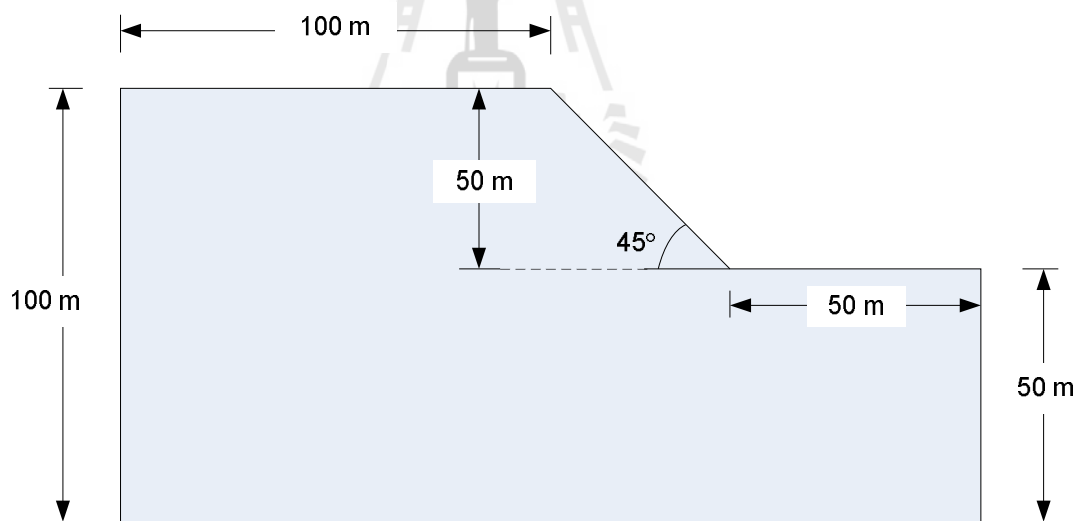
Before performing the computer analysis, physical and mechanical properties of rock samples are specified in the calculation. The major constants in the models are density, friction angle and cohesion of the rock slope. Table 5.1 gives the summary of the parameters used in computer simulation.

### **5.3 Computer model analysis**

The peak shear strength at higher shearing rate will result in a higher factor of safety and stability. The peak shear strength for low shearing rates and residual shear strength, results in a lower factor of safety and stability. This study uses slope height of 50 m and slope face angle is 45 degrees in a dry slope (Figure 5.1). Figures 5.2 through 5.4 show result of computer simulation for PW sandstone. The computer simulations using results from high and low shearing rates of the residual shear strengths (Table 5.1). Figures 5.5 through 5.7 show result of computer simulation of

**Table 5.1** Summary of the basic mechanical properties.

Rock type	Density (kg /m <sup>3</sup> )	Cohesion, c (MPa)			Friction angle, $\phi$ (degrees)		
		$\frac{\delta\tau}{\delta t}$ $2 \times 10^{-1}$ (MPa/s)	$\frac{\delta\tau}{\delta t}$ $2 \times 10^{-5}$ (MPa/s)	residual	$\frac{\delta\tau}{\delta t}$ $2 \times 10^{-1}$ (MPa/s)	$\frac{\delta\tau}{\delta t}$ $2 \times 10^{-5}$ (MPa/s)	residual
PWSS	2,250	0.61	0.003	0.002	51	45	39
PKSS	2,530	0.48	0.002	0.001	46	38	38
PPSS	2,410	0.49	0.006	0.001	53	44	32

**Figure 5.1** Slope model for computer simulation.

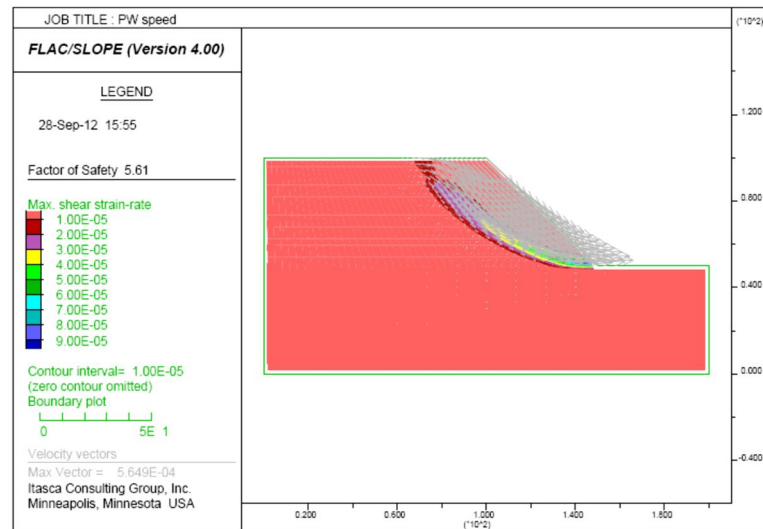


**Figure 5.2** Computer simulations of PW sandstone by using mechanical properties from shearing rate of  $2 \times 10^{-1}$  MPa/s.

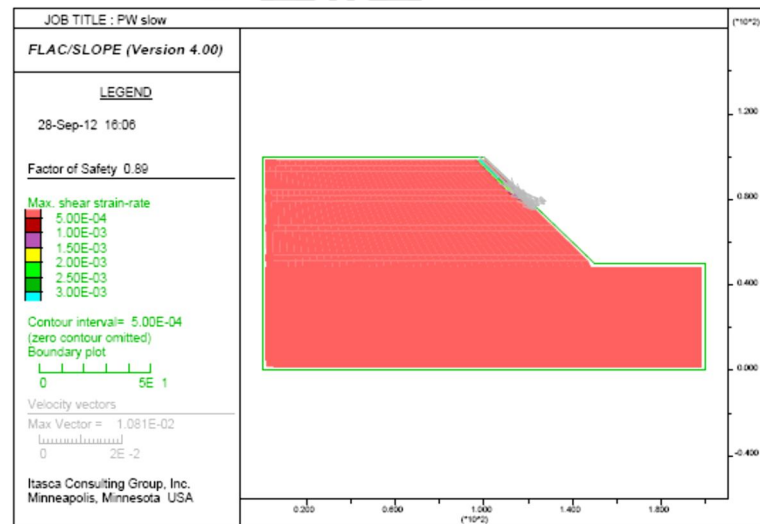


**Figure 5.3** Computer simulations of PW sandstone by using mechanical properties from shearing rate of  $2 \times 10^{-5}$  MPa/s.



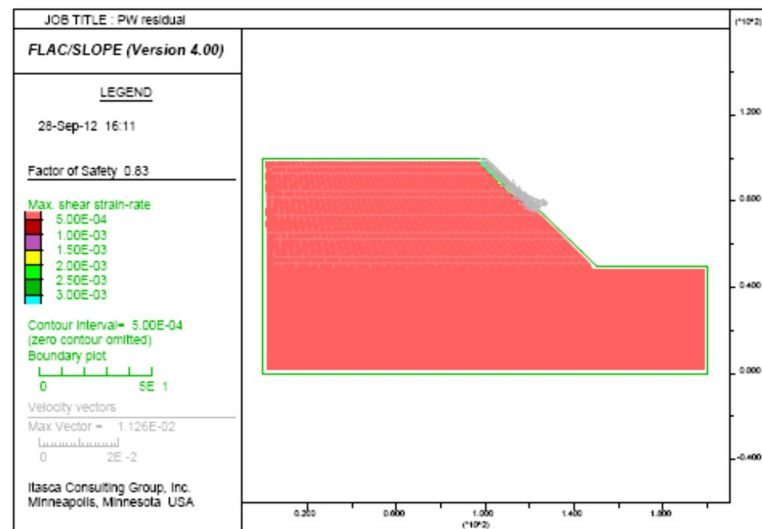


**Figure 5.4** Computer simulation of PW sandstone by using mechanical properties of residual strength.

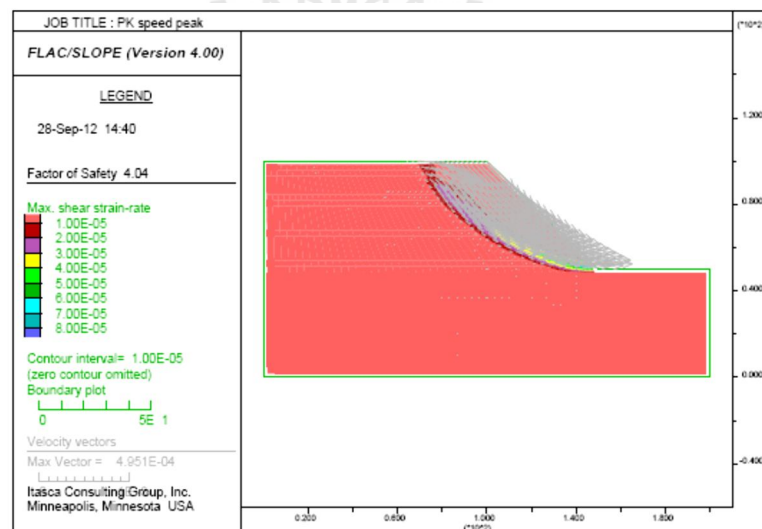


**Figure 5.5** Computer simulations of PK sandstone by using mechanical properties from shearing rate of  $2 \times 10^{-1}$  MPa/s.

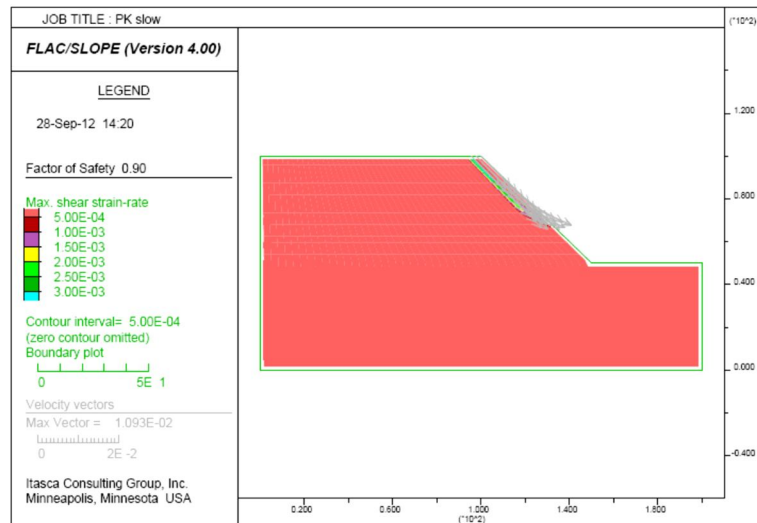


**Figure 5.6** Computer simulations of PK sandstone by using mechanical properties from shearing rate of  $2 \times 10^{-5}$  MPa/s.

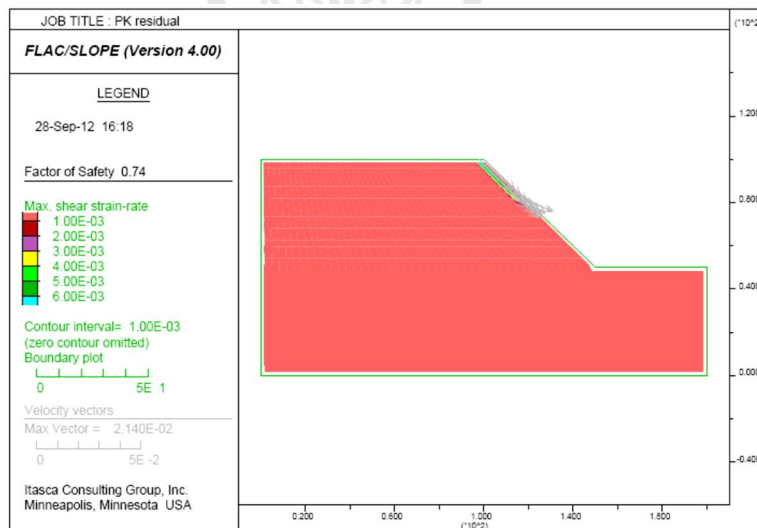


**Figure 5.7** Computer simulation of PK sandstone by using mechanical properties of residual strength.

PK sandstone. Figures 5.8 through 5.10 show result of computer simulation of PP sandstone. Table 5.2 gives summary of the factor of safety from computer simulations. The shear stresses at standard shearing rate will result in higher shear strength of the fracture, and hence higher factor of safety. The low shearing rate will give the results similar to the long-term strength of the fracture. This represents a more conservative analysis and design of the slope embankments.

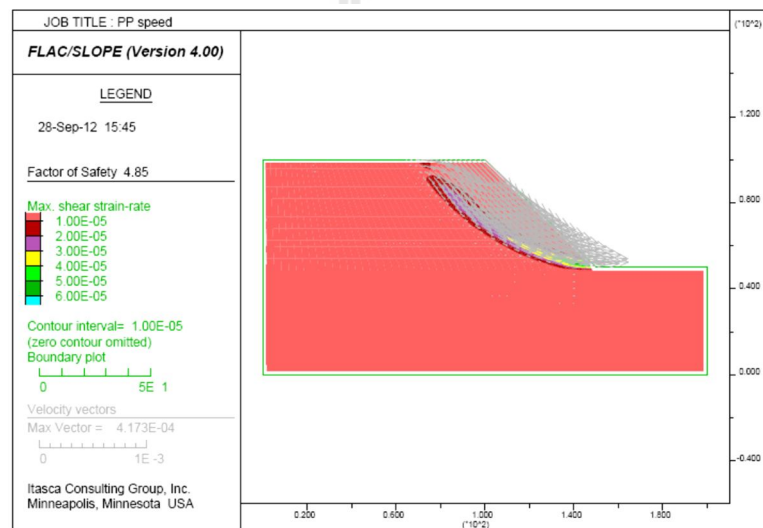


**Figure 5.8** Computer simulations of PP sandstone by using mechanical properties from shearing rate of  $2 \times 10^{-1}$  MPa/s.

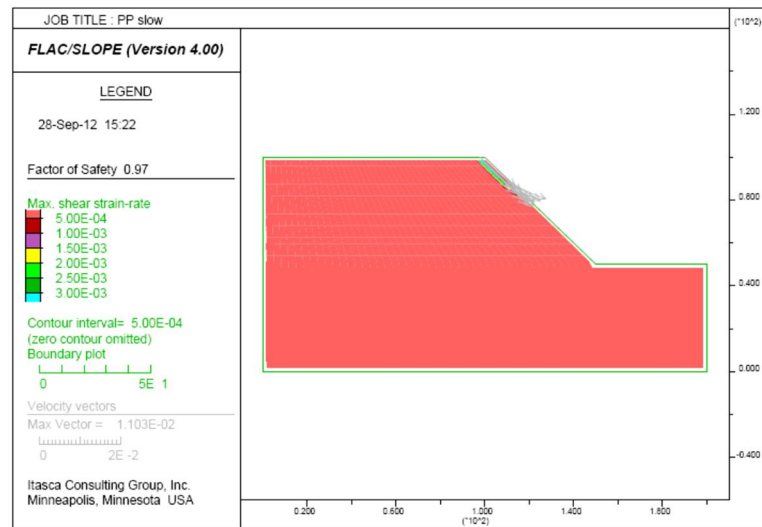


**Figure 5.9** Computer simulations of PP sandstone by using mechanical properties from shearing rate of  $2 \times 10^{-5}$  MPa/s.

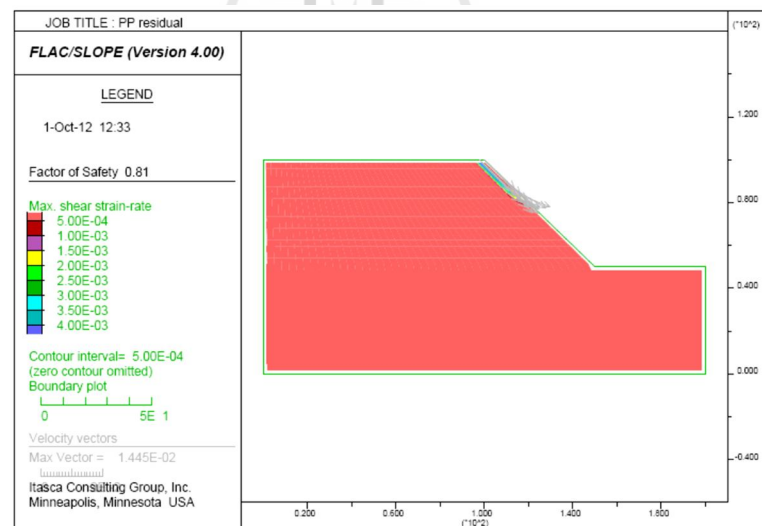
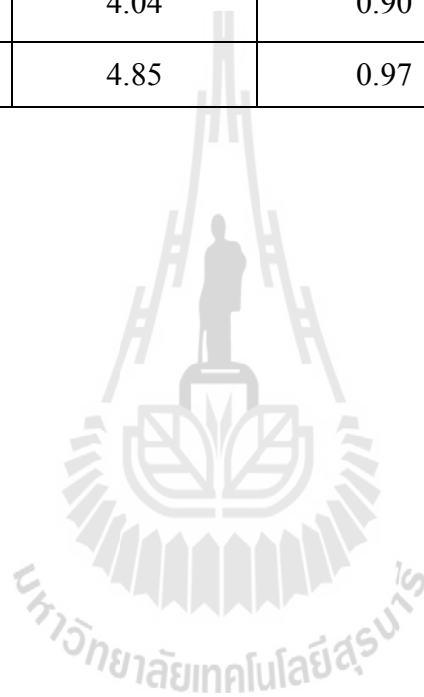


**Figure 5.10** Computer simulation of PP sandstone by using mechanical properties of residual strength.

**Table 5.2** Summary of the factors of safety from computer simulations.

Rock type	Factor of safety		
	Shear Rate $2 \times 10^{-1}$ (MPa/s)	Shear Rate $2 \times 10^{-5}$ (MPa/s)	residual
PW sandstone	5.61	0.99	0.83
PK sandstone	4.04	0.90	0.74
PP sandstone	4.85	0.97	0.81



# CHAPTER VI

## DISCUSSIONS, CONCLUSIONS, AND RECOMMENDATIONS FOR FUTURE STUDIES

### 6.1 Discussions and Conclusions

The shear rate can affect the shear strengths of the tension-induced fractures in the PP, PW and PK sandstones. Here the Coulomb's criterion can well describe the joint shear strengths of the rocks under the loading rates ranging from  $2 \times 10^{-5}$  to  $2 \times 10^{-1}$  MPa/s with the normal stresses from 0.2 to 4 MPa. The higher the loading rate applied, the higher the peak and residual shear stresses are obtained particularly under high normal stresses. Since the JRC values for all specimens of each sandstone type are in a narrow range (6 to 12) it is assumed that the roughness of the intension-induced fractures is the same for each sandstone type. As a result the cohesion and friction angle obtained for the Coulomb criterion can be correlated among different shear rates. It is found that both cohesion and friction angle notably increase with the shear rate. The cohesion can be as low as zero under the shear rate of  $2 \times 10^{-5}$  MPa/s to about 0.5-0.6 MPa under the shear rate of  $2 \times 10^{-1}$  MPa/s. The friction angles can increase by about 5 degrees when the shear rates increase from  $2 \times 10^{-5}$  to  $2 \times 10^{-1}$  MPa/s. The joint shear stiffness also increases with the shear rate. The scattering of the data is probably due to the intrinsic variability of the tested fracture.

The shear strengths of the saw cut surfaces are clearly independent of the shear rates. This suggests that the rate-dependent shear strength and stiffness of the

tension-induced fractures is primarily due to the time-dependent strength of the rock asperities on the fracture wall. This is supported by the experimental results obtained by Fuenkajorn and Khenkhunthod (2010) who conclude that the uniaxial and triaxial compressive strengths and elastic modulus of the three sandstones increase exponentially with the loading rate. It can therefore be postulated that the time-dependent shear strengths of the fractures may be found in other rock types of which compressive strengths are sensitive to loading rate.

## **6.2 Recommendations for future studies**


More rock samples should be tested under a wider range of normal stress. Different friction may be applied. The results will be very useful to construct a general empirical rock to quantify and determine the effect of shear rate on the friction of rock joints. It is also desirable to correlate the scale effect and time-dependent effect of the intact rock strength with the rate-dependent shear strength of the joints.

## REFERENCES

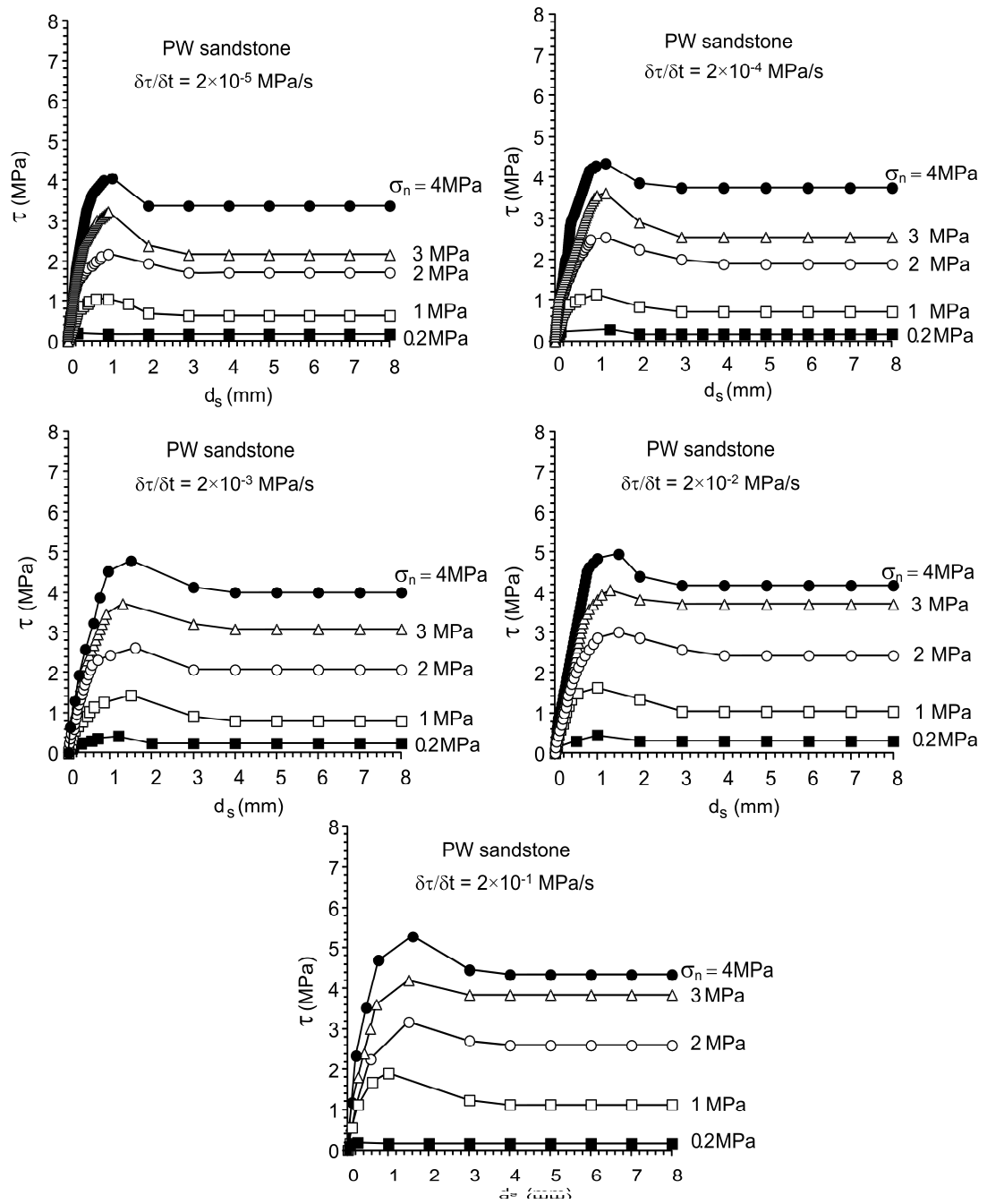
- ASTM D 5607-08. Test method for performing laboratory direct shear strength tests of rock specimens under constant normal force. **Annual Book of ASTM Standards**. 04.08. West Conshohocken: American Society for Testing and Materials: Philadelphia.
- Barton, N. (1973). Review of a new shear-strength criterion for rock joints. **Engineering Geology**. 7(4): 287-332.
- Crawford, A. M. and Curran, J. H. (1981). The influence of shear velocity on the frictional resistance of rock discontinuities. **International Journal of Rock Mechanics and Mining Sciences & Geomechanics**. 18(6): 505-515.
- Fuenkajorn, K. and Kenkhunthod, N. (2010). Influence of loading rate on deformability and compressive strength of three Thai sandstone. **Geotechnical and Geological Engineering**. 28(5): 707-715.
- Itasca (1994). **User Manual for FLAC-Fast Lagrangian Analysis of Continua**, Version 4.0. Itasca Consulting Group Inc. Minneapolis, Minnesota.
- Jafari, M.K., Hosseini, K. A., Boulon, M., Pellet, F., Jalaly, H., Uromeihy, A. and Buzzy, O. (2002). Laboratory investigation on shear strength variation of joint replicas due to low and high amplitude cyclic displacements. **Journal of Seismology and Earthquake Engineering** 4 (2-3): 37-49.
- Jafari, M.K., Hosseini, K.A., Pellet, F., Boulon, M. and Buzzi, O. (2003). Evaluation of shear strength of rock joints subjected to cyclic loading. **Soil Dynamics and Earthquake Engineering** 23 (7): 619-630.



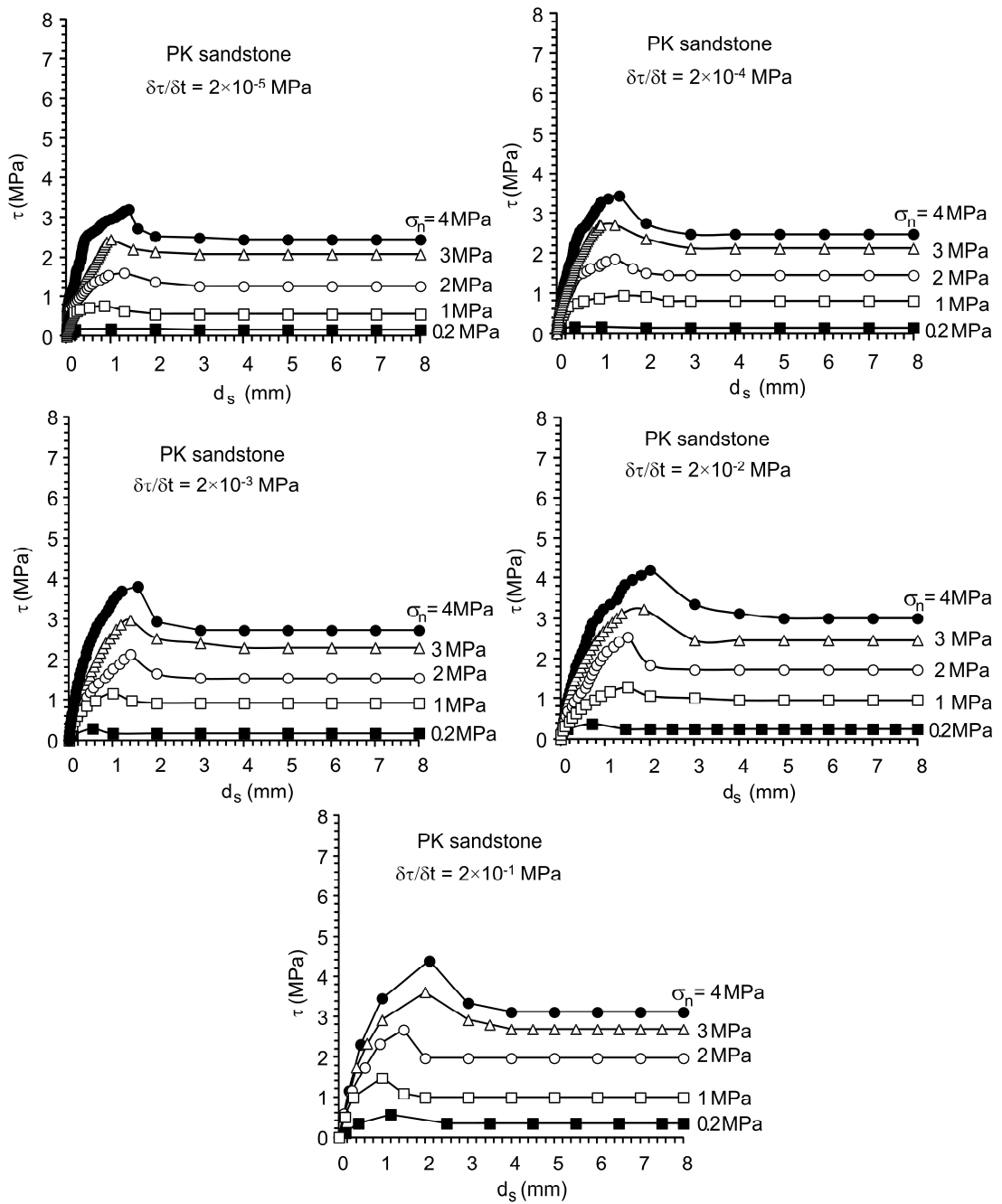
- Kemeny, J. (2003). The Time-Dependent Reduction of Sliding Cohesion due to Rock Bridges Along Discontinuities: A Fracture Mechanics Approach. **Rock Mechanics and Rock Engineering** 36 (1): 27-38.
- Kemthong, R. and Fuenkajorn, K. (2007). Prediction of joint shear strengths of ten rock types using field-identified parameters. **Proceedings of the First Thailand Symposium on Rock Mechanics**, Khao Yai, Thailand, Geomechanics Research Unit, Institute of Engineering Suranaree University of Technology, Thailand pp.195-209.
- Kwafniewskil; M.A. and Wang, J.A. (1997). Surface roughness evolution and mechanical behavior of rock joints under shear. **International Journal of Rock Mechanics & Mining Sciences** 34 (3-4): 157.e1-157.e14.
- Lee, H.S., Park, Y.J., Cho, T.F. and You, K.H. (2001). Influence of asperity degradation on the mechanical behavior of rough rock joints under cyclic shear loading. **International Journal of Rock Mechanics & Mining Sciences** 38 (7): 967-980.
- Park, J.W. and Song, J.J. (2009). Numerical simulation of a direct shear test on a rock joint using a bonded-particle model. **International Journal of Rock Mechanics & Mining Sciences** 46 (8): 1315-1328.
- Seidel, J.P. and Haberfield, C.M. (2002). A Theoretical Model For Rock Joints Subjected To Constant Normal Stiffness Direct Shear. **International Journal of Rock Mechanics and Mining Sciences** 39 (5): 539-553.
- Vasarhelyi, B. (1998). Influence of normal load on joint dilatation rate. **Rock Mechanics and Rock Engineering** 31 (2): 117-123.



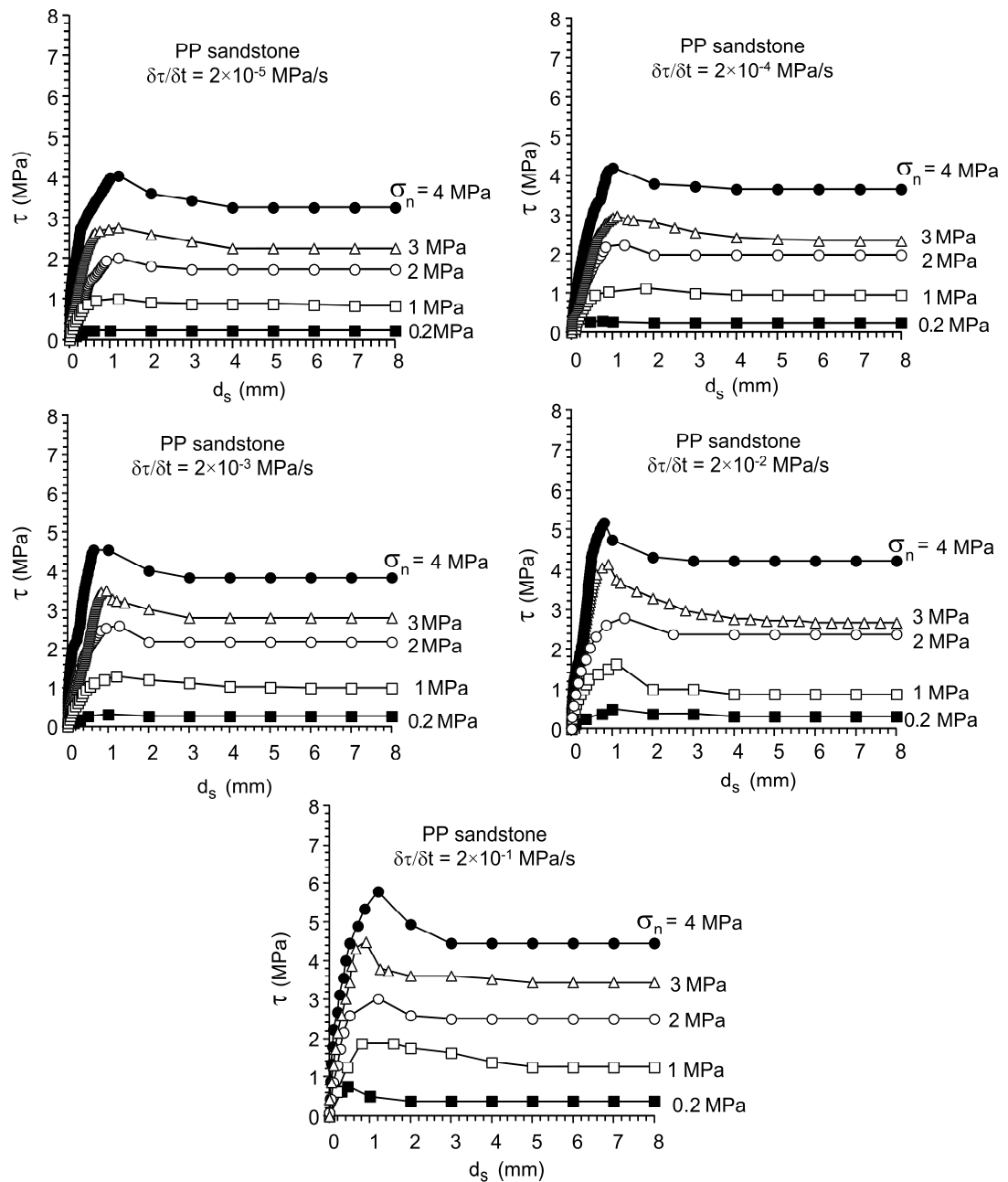
**APPENDIX A**  
**SHEAR STRESS-DISPLACEMENT CURVES FROM**  
**DIRECT SHEAR TESTS**



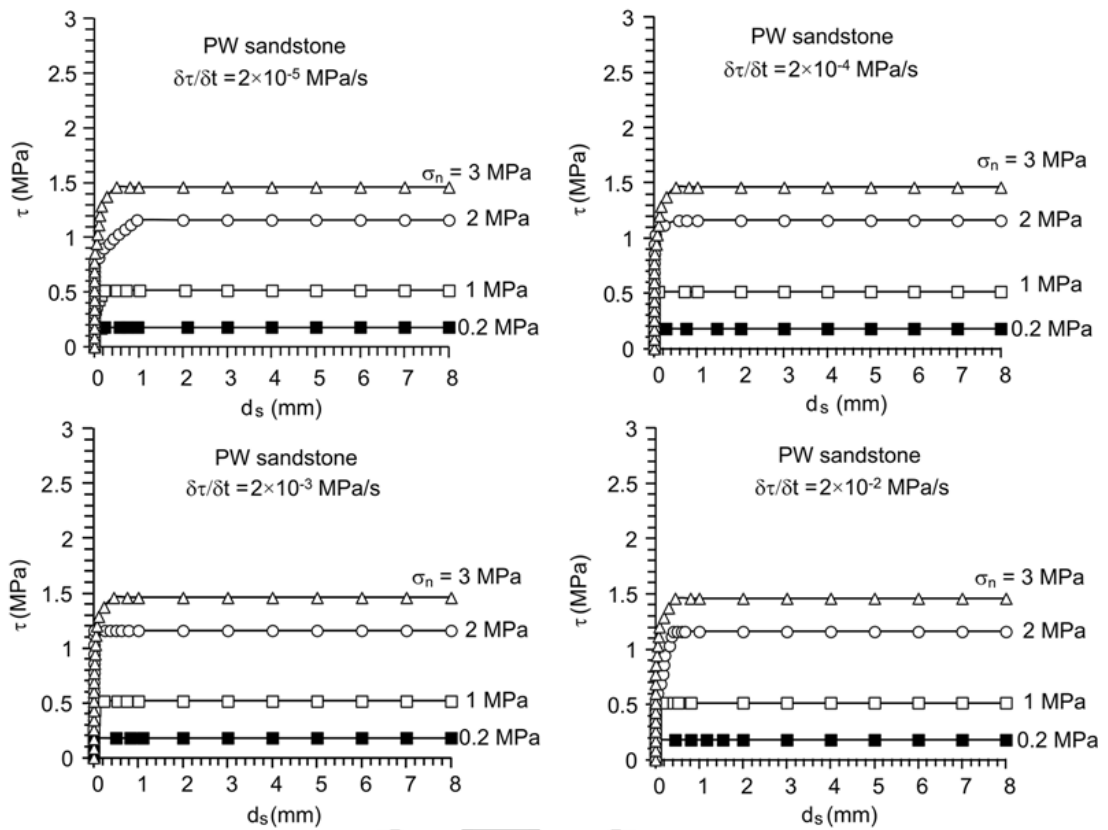
**Figure A.1** Shear stress of PW sandstone as a function of displacement.



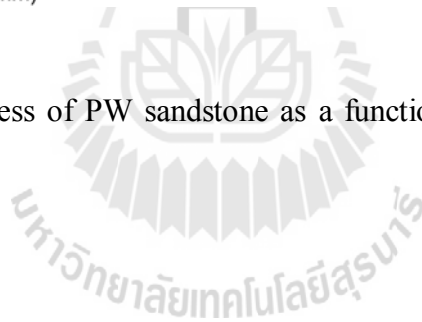
**Figure A.2** Shear stress of PK sandstone as a function of displacement.



**Figure A.3** Shear stress of PP sandstone as a function of displacement.



**Figure A.4** Shear stress of PW sandstone as a function of displacement on saw cut surface.



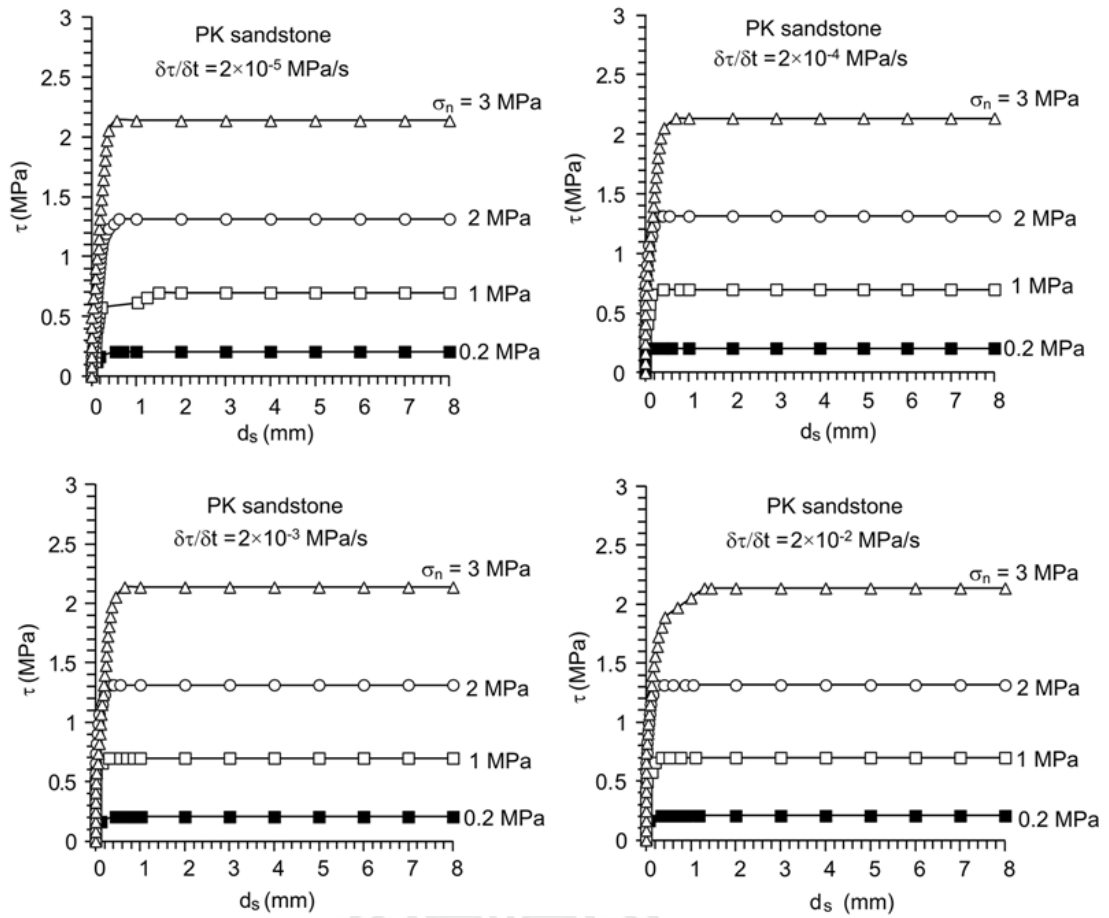


**Figure A.5** Shear stress of PK sandstone as a function of displacement on saw cut surface.

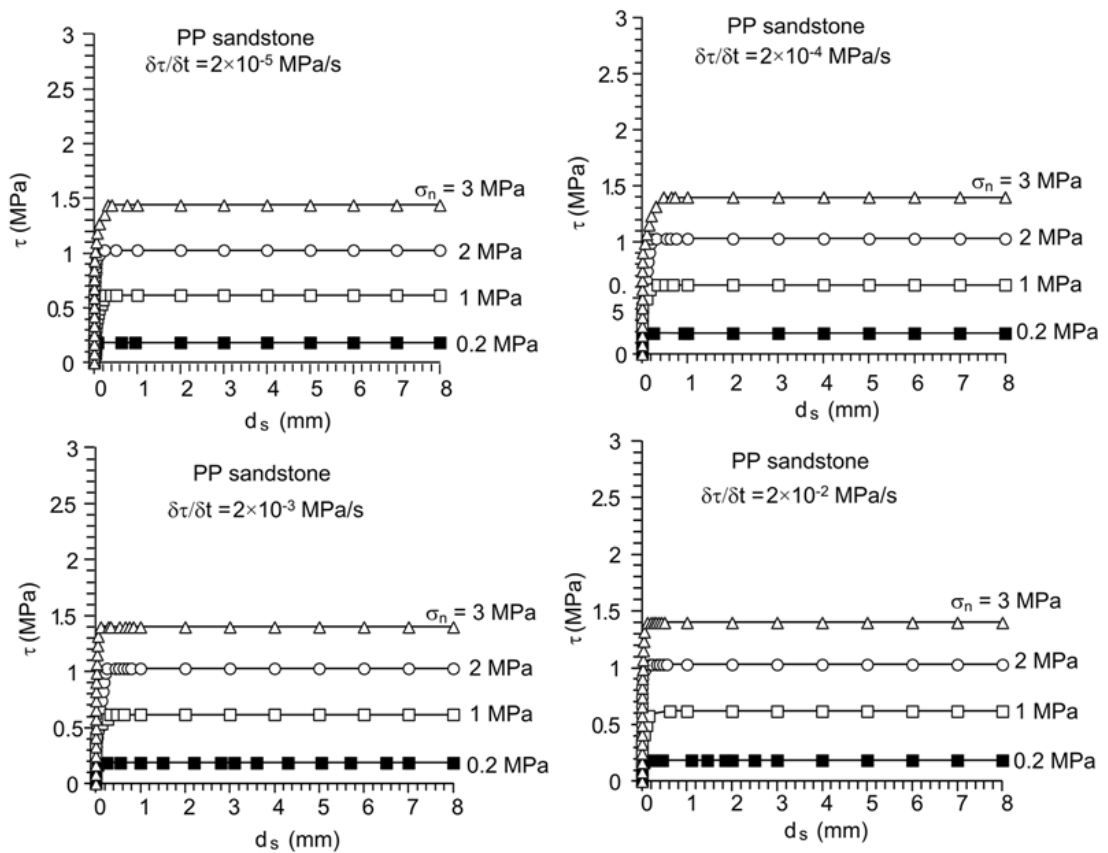


**Figure A.6** Shear stress of PK sandstone as a function of displacement on saw cut surface.